BODIPY-based Regioisomers and Donor-Acceptor Rotor as Organic Photosensitizers for Maximizing Singlet Oxygen Quantum Yields and for Photooxidation of Thioanisole

Sushil Sharma[a], Sakshi Chawla[a], Vidushi Gupta[a], Arijit K. De[a*] and Sanchita Sengupta[a*]

Department of Chemical Sciences, Indian Institute of Science Education and Research (IISER) Mohali, Knowledge City, Sector 81, P.O. Manauli, Mohali, Punjab 140306, India.

*E-mail: sanchita@iisermohali.ac.in, akde@iisermohali.ac.in

Table of contents

1. Materials and Methods:

All chemicals and solvents were purchased from commercial suppliers (Sigma Aldrich, SD Fine Chemicals) and used without further purification. Toluene (Tol) was dried over sodium/benzophenone and distilled prior to use. *N*, *N*-dimethylformamide (DMF) was dried over calcium hydride and distilled prior to use. Silica gel of mesh size 60-120 was used for column chromatography. The ^{1}H and ^{13}C NMR spectra were recorded on a 400 MHz Bruker Biospin Avance III FT-NMR spectrometer, respectively with TMS as standard at room temperature. The solvent used was $CDCl_3$ (from Merck, Germany) and all the spectra were recorded in $CDCl_3$ and dimethyl sulfoxide-d_6 (DMSO) with TMS as the internal standard.

Mass spectrometry measurements were performed on UltrafleXtreme MALDI TOF/TOF (Bruker Daltonics) instrument. Software used for acquiring mass spectra was Flex Control, Bruker (USA) and software used for analyzing mass spectra was Flex Analysis 3.1.

All spectroscopic measurements were performed at room temperature unless otherwise mentioned. UV/Vis spectra were recorded on Cary 60 UV/Vis spectrophotometer using a quartz cuvette with 1 cm path length. Fluorescence solution measurements were performed with Hitachi F7000 fluorescence spectrophotometer equipped with R928F photomultiplier expandable up to 900 nm. Various excitation wavelengths were used to perform the fluorescence measurements. Standard software FL Solutions was used for the measurement and analysis of the data.

Electrochemical measurements were performed using CHI-610E electrochemical workstation from CH Instruments (USA), with a conventional three electrode single-compartment cell consisting of a glassy carbon as the working electrode, Ag/AgCl containing 3M KCl solution as the reference electrode, and Pt wire as the counter electrode. Cyclic voltammetry measurements were performed at a scan-rate of 0.1 V/s. As a supporting electrolyte, 0.1 M tetrabutylammonium hexafluorophosphate (TBAHPF) (Alfa Aesar) dissolved in pre-dried DCM was used. The solutions were purged with nitrogen for 2 mins prior to measurement. The concentration of the prepared samples was ~ 0.1-0.3 mM. The electrochemical potential was internally calibrated against the standard ferrocene/ferrocenium (Fc/Fc^{+}) redox couple.

Temperature-dependent fluorescence of samples were measured using temperature-controlled cuvette holder for Hitachi F7000 spectrophotometer (Luma 40) from Quantum Northwest. The Luma 40 was used for temperature range of -20 ^{o}C to +100 ^{o}C.

The electron paramagnetic resonance (EPR) studies were performed using Jeol JES320 spectrometer and 5,5-dimethyl-1-pyrroline 1-oxide (DMPO) as the spin trapper.

Time resolved fluorescence spectra were measured using time correlated single photon counting (TCSPC) model from Fluorocube, Horiba Jobin Yvon, NJ equipped with picosecond laser diodes as excitation source. The 375 nm laser diode was used as a light source for the excitation of samples and the instrument response function (IRF) was collected using Ludox (colloidal silica) solution. The width (FWHM) of IRF was ~ 250 ps. The optical pulse durations from < 70ps were used. Highly integrated picosecond PMT modules as well as micro channel plate PMTs were used for the time resolution.

Quantum chemical density functional theory (DFT), TD-DFT and NTO calculations were performed for ***pp*-BODIPY**, ***mp*-BODIPY**, ***mm*-BODIPY**, **T-BODIPY** and **T-ADA** in ground state using Gaussian09 program suite. [S1] The side chains in all molecules were replaced with methyl group in order to account for the electron donating effect of the alkyl chain and at the same time reducing the computational time and cost. The studied molecules were optimized using global hybrid B3LYP functional and 6–31G (d, p) basis set in gas phase. The frontier molecular orbitals (FMO) electronic levels and FMO distribution were obtained from geometry optimization into neutral ground state geometries. FMO percentage contribution analysis was performed using GaussSum version 3 software. First single point calculations were performed at the B3LYP/6-31G(d,p) level with the keywords pop=full iop (3/33=1,3/36=–1) and the output file was analyzed by GaussSum to obtain the FMO composition analysis of the donor and acceptor of all molecules.

2. Synthesis

Synthesis of 4-bormo[1,1'-biphenyl]-4-carbaldehyde (1)

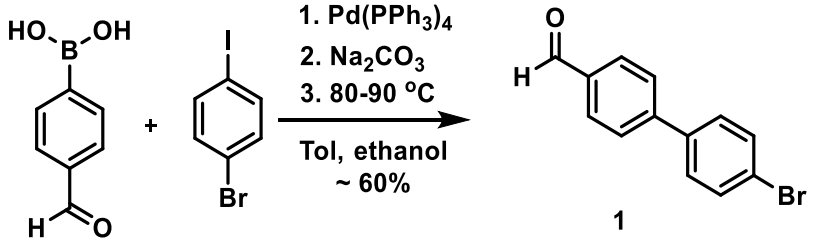

Scheme S1. Synthesis of 4-bormo[1,1'-biphenyl]-4-carbaldehyde (1).[S2]

Procedure: 4-formyl phenyl boronic acid (1 gm, 6.669 mmol) in 20 mL ethanol and 1-bromo-4-iodobenzene (2.018 gm, 7.135 mmol) in 20 mL Tol was taken in Schlenk tube and degassed

through freeze-pump-thaw several times. In two neck round-bottomed flask, $Pd(PPh_3)_4$ (3-5 mol%), was taken and simultaneously 4-formyl phenyl boronic acid,1-bromo-4-iodobenzene and 2 M solution of Na_2CO_3 were added and stirred for overnight at 80-90 °C. The reaction mixture was cooled and extracted by ethyl acetate and pass-through sodium sulphate. The final compound was purified by column chromatography using ethyl acetate and hexane (10:90, v/v). The final compound was obtained as white solid with 60% yield.

^{1}H NMR (400 MHz, $CDCl_3$): δ 10.06 (s, 1 H), 7.95 (d, J = 8 Hz, 2 H), 7.72 (d, J = 8 Hz, 2 H), 7.61 (d, J = 8 Hz, 2 H), 7.50 (d, J = 8 Hz, 2 H).

Synthesis of 3- bromobipheny4- carbaldehyde (2)

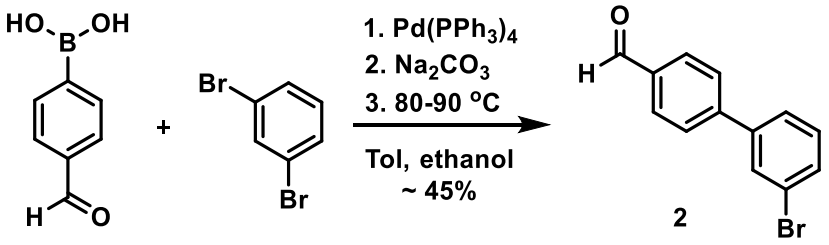

Scheme S2. Synthesis of 3- bromobipheny4- carbaldehyde (2). [S2]

Procedure: 4-formyl phenyl boronic acid (100 mg, 0.66 mmol) in 5 mL ethanol and 1, 3-dibromobenzene (120 mg, 0.42 mmol) in 5 mL Tol was taken in Schlenk tube and degassed through freeze-pump-thaw several times. In two neck round-bottomed flask, $Pd(PPh_3)_4$ (3-5 mol%), was taken and simultaneously 4-formyl phenyl boronic acid, 1, 3-dibromobenzene and 2 M solution of Na_2CO_3 were added and stirred for overnight at 80-90 °C. The reaction mixture was cooled and extracted by ethyl acetate and pass-through sodium sulphate. The final compound was purified by column chromatography using ethyl acetate and hexane (10:90, v/v). The pure oily compound was obtained with 45% yield.

^{1}H-NMR (400 MHz, $CDCl_3$): δ 10.05 (s, 1 H), 7.95 (d, J = 8 Hz, 2 H), 7.76 (d, J = 4 Hz, 1 H), 7.70 (d, J = 8 Hz, 2 H), 7.54 (d, J = 8 Hz, 2 H), 7.34 (t, J = 8 Hz, 1 H).

Synthesis of 3-bormo[1,1'-biphenyl]-3-carbaldehyde (3)

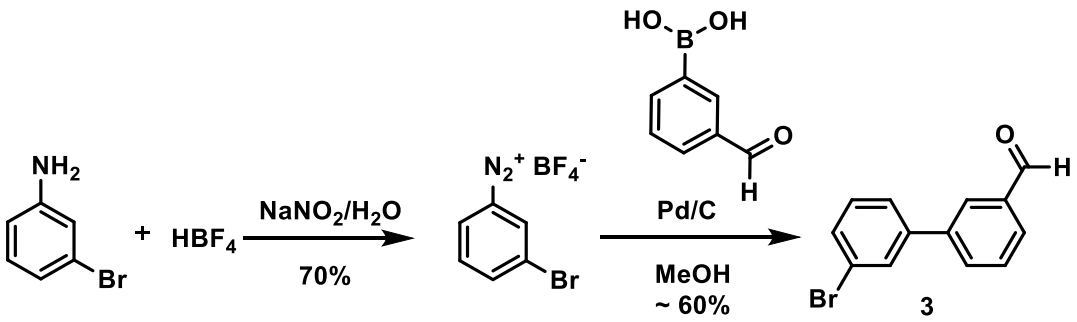

Scheme S3. Synthesis of 3-bormo[1,1'-biphenyl]-3-carbaldehyde (3) [S3].

Procedure: 3-Bromoaniline (0.32 mL, 2.906 mmol) was added in HBF_4 (1.2 mL) at room temp. An aqueous solution of sodium nitrite (200 mg $NaNO_2$) in 0.5 mL water was added dropwise at 0 °C over 5 min. The resulting mixture was stirred for 40 min. at 0 °C and the formed precipitate was filtered out and dried. The precipitate was re-dissolved in minimum amount of acetone and then diethyl ether was added to the solution until precipitate formed. The obtained precipitate was filtered off and washed several times with diethyl ether and dried at high vacuum. The pure brown solid was obtained with 70% yield.

Diazonium salt (325 mg, 1.2 mmol), 3-formyl phenyl boronic acid (150 mg, 1 mmol) and Pd/C (6 mg, 0.05 mmol) was dissolved in MeOH and then the reaction mixture was stirred at 50 ^{o}C until the evolution of nitrogen stopped. Then the reaction mixture was cooled and filtered through celite pad using ethyl acetate. The solvent was evaporated on rota-vapour and the compound was purified by column chromatography using ethyl acetate and hexane (10:90, v/v). The pure white solid compound was obtained with 60% yield.

^{1}H-NMR (400 MHz, $CDCl_3$): δ 10.08 (s, 1 H), 8.06 (s, 1 H), 7.88 (d, J = 8 Hz, 1 H), 7.82 (dt, J = 8, 1.7 Hz, 1 H), 7.76 (t, J = 4 Hz, 1 H), 7.62 (t, J = 8 Hz, 1 H), 7.53 (t, J = 8 Hz, 2 H), 7.34 (t, J = 78 Hz, 1 H).

Synthesis of *pp*-BODIPY

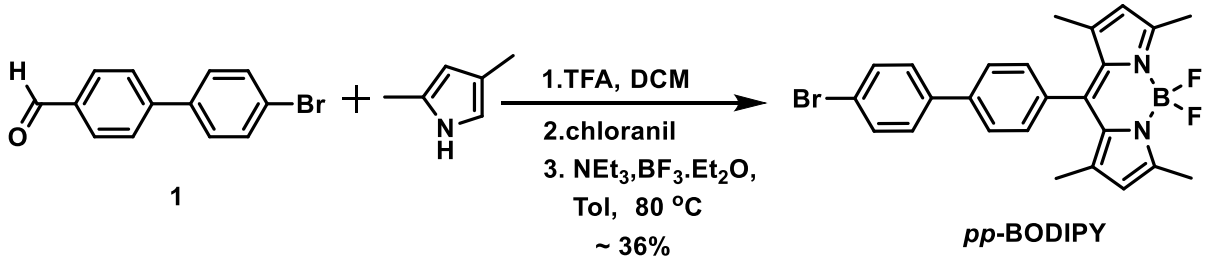

Scheme S4. Synthesis of ***pp*-BODIPY**. [S4]

Procedure: 4-Bromobiphenyl-4-carbaldehyde (1) (100 mg, 0.38 mmol) was taken in dry dichloromethane (DCM) in two neck round bottomed flask and purged with nitrogen. Then 2,4-dimethylpyrrole (127 mg, 1.34 mmol) was added in dark condition and subsequently 3 or 4 drops of TFA was added and the reaction was stirred for 5 h at room temp monitored by thin layer chromatography (TLC). Then chloranil (102 mg, 0.417 mmol) was added to the reaction mixture and stirred for 40 minutes at room temperature. Then the reaction mixture was subjected to flash column chromatography using DCM as eluent and the solvent was evaporated and dried. Subsequently, dry Tol was added to reaction mixture and triethylamine (NEt_3) (776 mg, 7.67 mmol) was added and allowed to stir for 15 min. Then boron trifluoride diethyl etherate ($BF_3 \cdot Et_2O$) (1.3 gm, 9.1 mmol) was added to the reaction mixture and stirred for 40 min at 80 °C. Then the reaction mixture was cooled and extracted using ethyl acetate and solvent was evaporated. The compound was purified by column chromatography using DCM and hexane (20:80, v/v). The pure red solid compound was obtained with 36% yield.

^{1}H-NMR (400 MHz, $CDCl_3$): δ 7.70 (d, J = 7.6 Hz, 2 H), 7.61 (d, J = 8.1 Hz, 2 H), 7.54 (d, J = 6.9 Hz, 2 H), 7.36 (d, J = 7.3 Hz, 2 H), 5.99 (s, 2 H), 2.57 (s, 6 H), 1.43 (s, 6 H).

ESI-TOF: $(M+H)^+$ of molecular formula $C_{25}H_{22}BBrF_2N_2$: Calculated 479.1105; found 479.2756.

Synthesis of *mp*-BODIPY

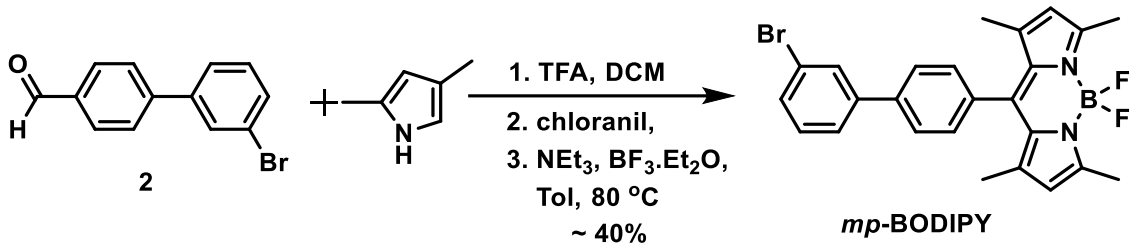

Scheme S5. Synthesis of ***mp*-BODIPY**. [S4]

Procedure: ***mp*-BODIPY** was synthesized using the same procedure as used in the synthesis of ***pp*-BODIPY**. The pure orange solid with 40% was obtained.

^{1}H-NMR (400 MHz, $CDCl_3$): δ 7.82 (s, 1 H), 7.71 (d, J = 7.5 Hz, 2 H), 7.60 (d, J = 7.7 Hz, 1 H), 7.52 (d, J = 7.3 Hz, 1 H), 7.37 (d, J = 7.3 Hz, 3 H), 6.00 (s, 2 H), 2.57 (s, 6 H), 1.43 (s, 7 H).

^{13}C NMR (100 MHz, $CDCl_3$): δ 155.81, 143.08, 142.19, 141.18, 140.72, 135.83, 131.46, 130.91, 130.60, 130.10, 129.92, 127.64, 127.55, 126.65, 125.68, 123.22, 121.46, 29.83, 14.71.

ESI-TOF: $(M+H)^+$ of molecular formula $C_{25}H_{22}BBrF_2N_2$: Calculated 479.1105; found 479.2756.

Synthesis of *mm*-BODIPY

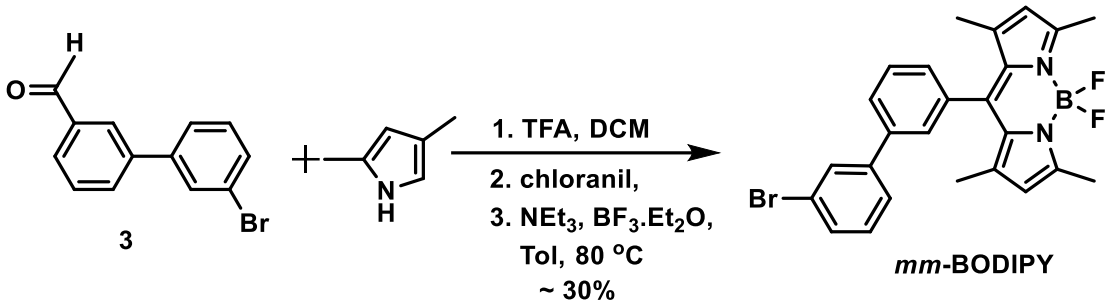

Scheme S6. Synthesis of ***mm*-BODIPY**. [S4]

Procedure: *mm*-BODIPY was synthesized using the same procedure as used in the synthesis of ***pp*-BODIPY**. The pure orange solid with 30% was obtained.

^{1}H-NMR (400 MHz, $CDCl_3$): δ 7.74 (s, 1 H), 7.69 (d, *J* = 8 Hz, 1 H), 7.58 (t, *J* = 8 Hz, 1 H), 7.55 – 7.48 (m, 3 H), 7.32 (t, *J* = 8 Hz, 2 H), 6.00 (s, 2 H), 2.57 (s, 6 H), 1.43 (s, 6 H).

^{13}C NMR (100 MHz, $CDCl_3$): *δ* 155.77, 143.17, 142.27, 140.39, 134.77, 130.89, 130.59, 130.30, 128.81, 127.80, 125.81, 124.92, 123.23, 29.85, 14.71.

ESI-TOF: $(M+H)^+$ of molecular formula $C_{25}H_{22}BBrF_2N_2$: Calculated 479.1105; found 479.2756.

Synthesis of methyl-pyrrole

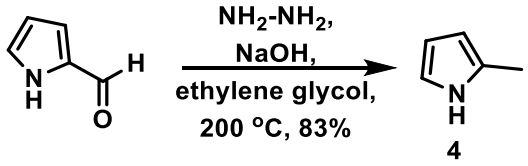

Scheme S7. Synthesis of methyl-pyrrole (4).[S5]

Procedure: Pyrrole-2-carboxyaledhyde (2 g, 21.03 mmol), NaOH (4.37 g, 109.36 mmol) and hydrazine hydrate (4.16 g, 129.97 mmol) was dissolved in ethylene glycol (40 mL) and then heated under nitrogen at 200 °C for 5 h. During the course of reaction, the organic phase was distilled using a Dean-Stark apparatus. The reaction mixture was extracted using brine solution (4 × 10 mL) and diethyl ether (3 × 10 mL) twice and then the organic layers were dried over anhydrous Na_2SO_4 and the solvent was evaporated via rotary evaporator. Pure compound was obtained in the form of yellow oily liquid with a yield of 83%.

^{1}H NMR (400 MHz, $CDCl_3$): δ 7.99 (s, 1 H), 6.73 (d, J = 4 Hz, 1 H), 6.26 (q, J = 4 Hz, 1 H), 6.04 (s, 1 H), 2.38 (s, 3 H).

Synthesis of T-BODIPY

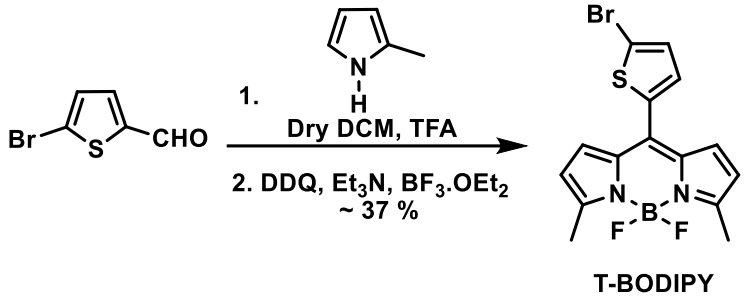

Scheme S8. Synthesis of **T-BODIPY**.[S6]

Procedure: To a solution of 5-bromo-2-thiophenecarbaldehyde (400 mg, 2.09 mmol) and 2-methylpyrrole (424 mg, 5.23 mmol) in dry dichloromethane (DCM) (40 mL) two drops of trifluoroacetic acid (TFA) was added under nitrogen, and the mixture was stirred at room temperature overnight. 2,3-dichloro-5,6-dicyano-1,4-benzoquinone (DDQ) (474 mg, 2.09 mmol) was added to the reaction mixture and stirred for additional 2.5 h at room temperature. Then Et_3N (1.27 g, 12.54 mmol) was added to the reaction mixture stirred for 15 minutes and then $BF_3{\cdot}Et_2O$ (1.19 g, 8.36 mmol) were added to the reaction mixture and stirred for 2 h. The reaction mixture was poured into water (4 × 10 mL) and extracted with DCM (8 × 10 mL). The combined organic layers were extracted 5 times and was then dried over Na_2SO_4, filtered and evaporated under vacuum using rotary evaporator to give a crude product, which was purified by column chromatography on silica gel using DCM/hexane (2/1, v/v) as the eluent. The pure product was obtained as a crystalline red solid with a yield of 37%.

^{1}H NMR (400 MHz, $CDCl_3$): δ (ppm) 7.17 (d, J = 4 Hz, 2 H), 7.04 (d, J = 4 Hz, 2 H), 6.31 (d, J = 4 Hz, 2 H), 2.64 (s, 6 H).

^{13}C NMR (100 MHz, $CDCl_3$): δ (ppm) 158.36, 136.19, 133.99, 133.37, 131.81, 130.77, 130.27, 119.88, 117.02, 29.84, 15.15.

ESI-TOF: $(M+K)^+$ of molecular formula $C_{15}H_{12}BBrF_2N_2S$: Calculated 418.9643; found 418.9643.

Synthesis of T-ADA

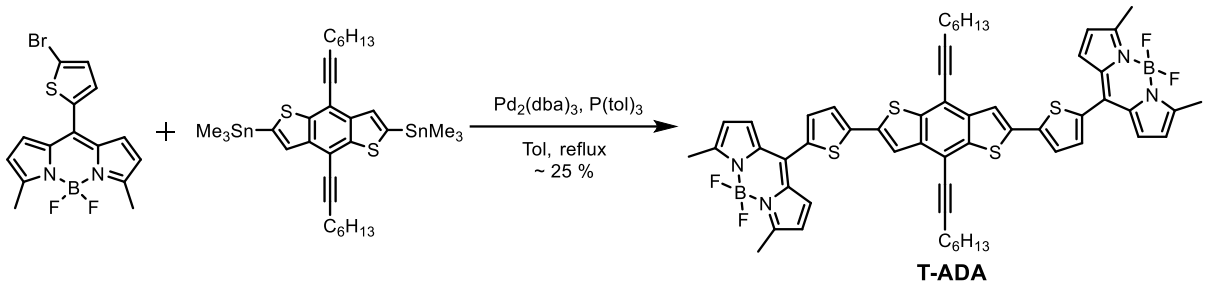

Scheme S9. Synthesis of **T-ADA**.[S7]

Procedure: BDT-$SnMe_3$ (70 mg, 0.095 mmol) and thiophene-BODIPY (91.45 mg, 0.24 mmol) were dissolved in toluene and degassed by freeze-pump-thaw method. In two neck round bottom flask, $Pd_2(dba)_3$ (2.1 mg, 0.002 mmol), $P(o\text{-}tol)_3$ (3.3 mg, 0.011 mmol) were taken and simultaneously BDT-$SnMe_3$ and thiophene-BODIPY was added and refluxed for 5 h. The reaction mixture was cooled and evaporate and purified by column chromatography using chloroform and hexane (80:20, v/v). The final compound was obtained as brown solid with 25% yield.

^{1}H NMR (400 MHz, $CDCl_3$): δ (ppm) 7.70 (s, 2 H), 7.43 (q, 4 H), 7.17 (d, J = 4 Hz, 4 H), 6.34 (d, J = 4 Hz, 4 H), 2.67 (s, 12 H), 1.78 (t, J = 8 Hz, 4 H), 1.43 (s, 10 H), 0.94 (t, J = 8 Hz, 6 H), 0.88 (t, J = 8 Hz, 6 H).

^{13}C NMR (100 MHz, $CDCl_3$): δ (ppm) 158.00, 141.86, 139.09, 137.28, 135.02, 133.99, 132.84, 130.66, 130.26, 129.11, 128.54, 126.02, 125.54, 120.30, 119.75, 112.07, 32.07, 31.53, 29.84, 29.51, 28.83, 22.84, 20.18, 15.17, 14.31.

ESI-TOF: $(M+H)^+$ of molecular formula : $C_{56}H_{52}B_2F_4N_4S_4$: Calculated 1007.3278; found 1007.3271.

3. ^{1}H NMR and ^{13}C NMR spectra

^{1}H NMR of 1:

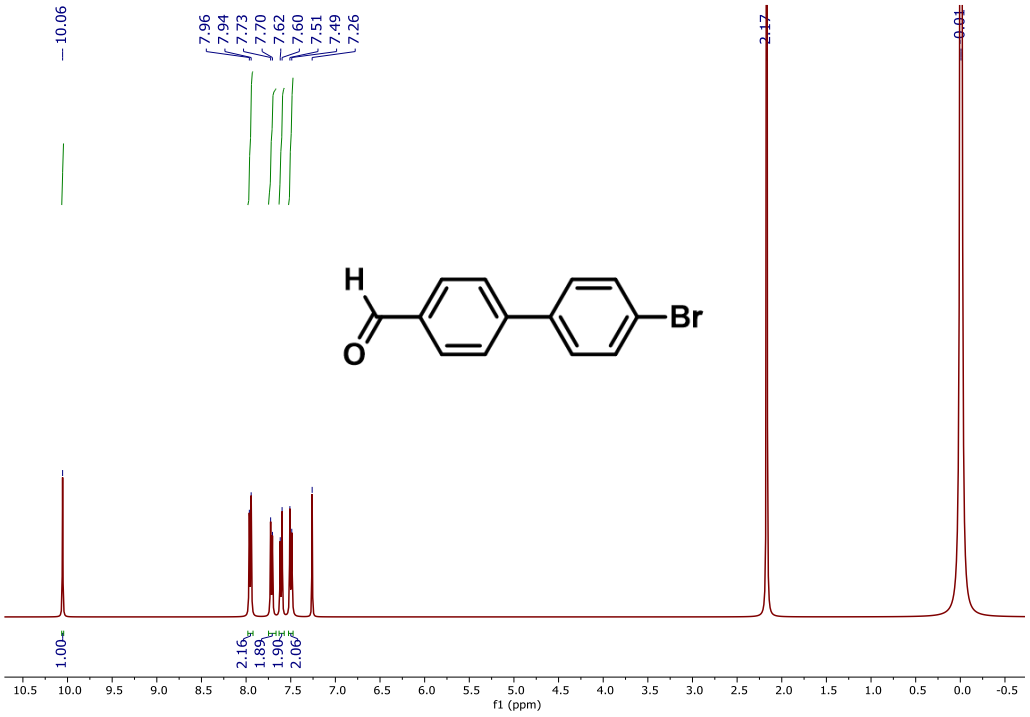

^{1}H NMR of 2:

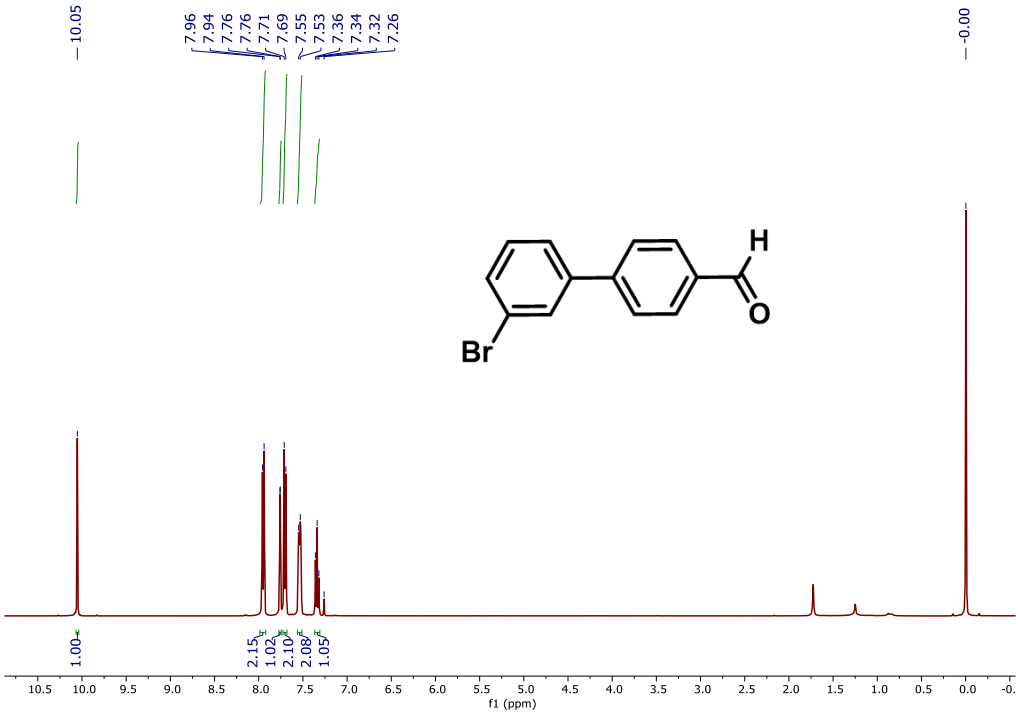

^{1}H NMR of 3:

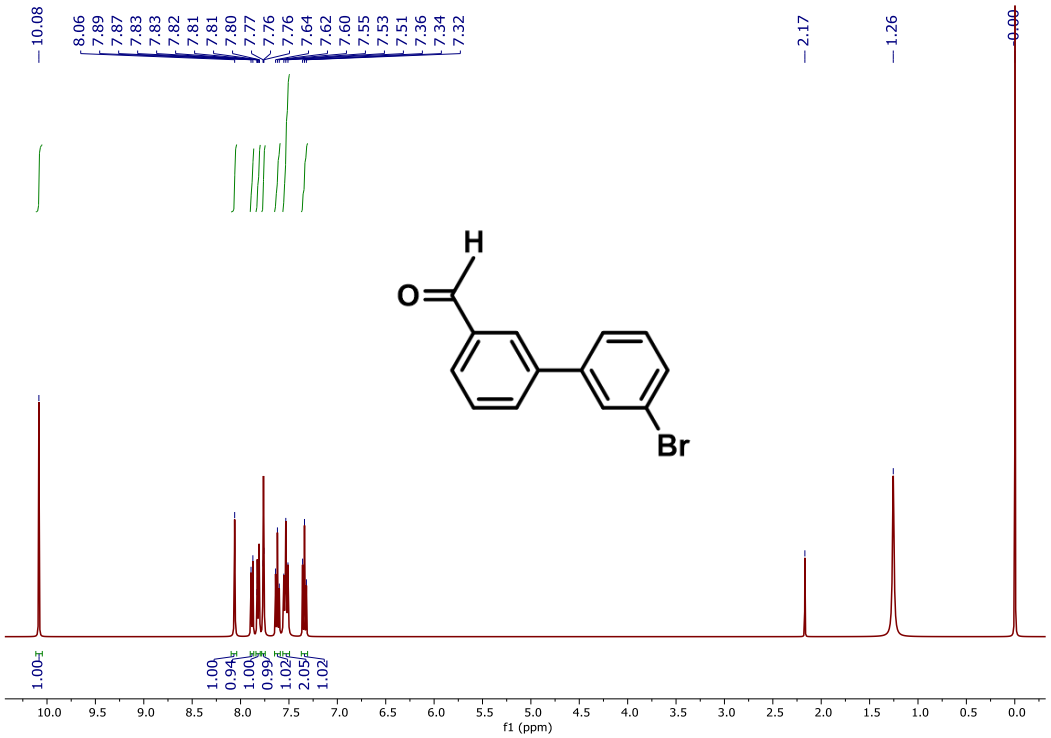

^{1}H NMR of *pp*-BODIPY:

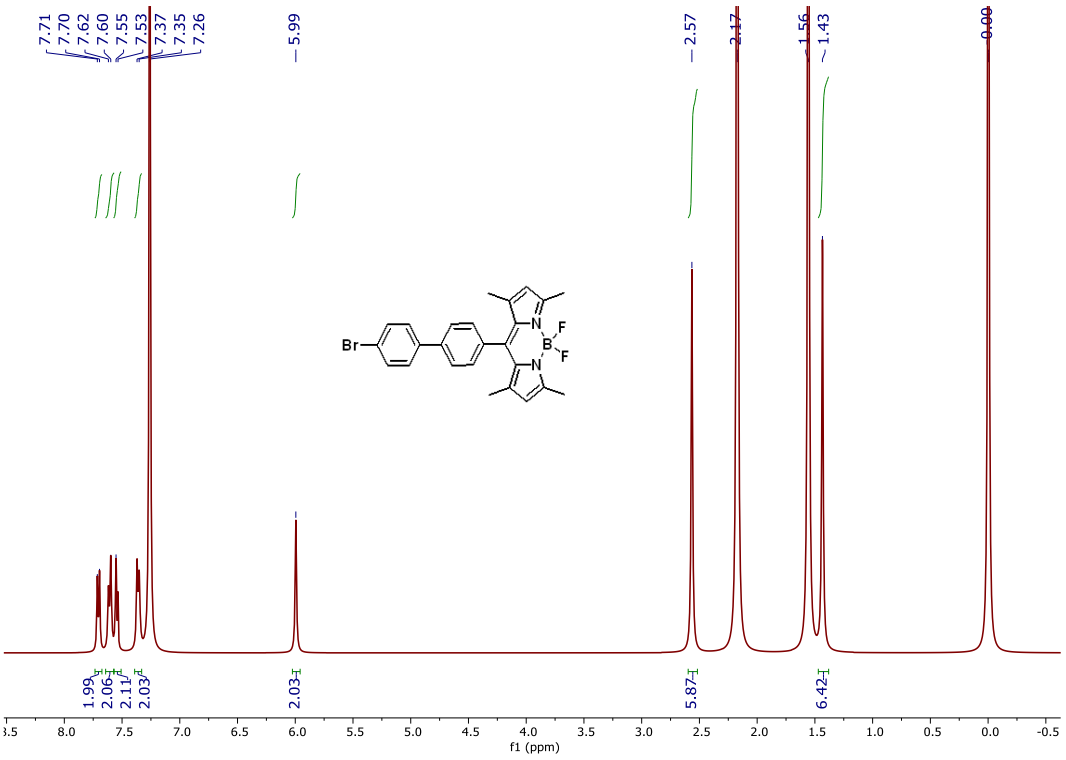

^{13}C NMR of *pp*-BODIPY:

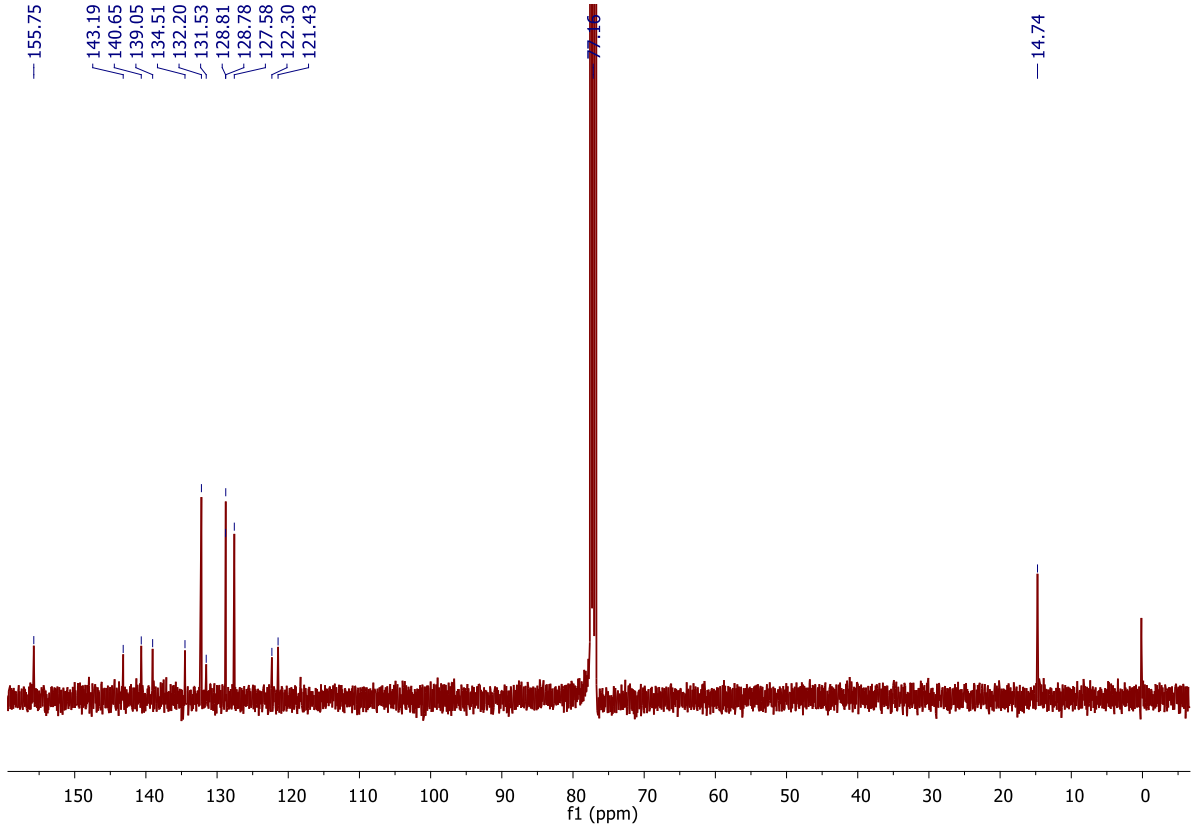

^{1}H NMR of *mp*-BODIPY:

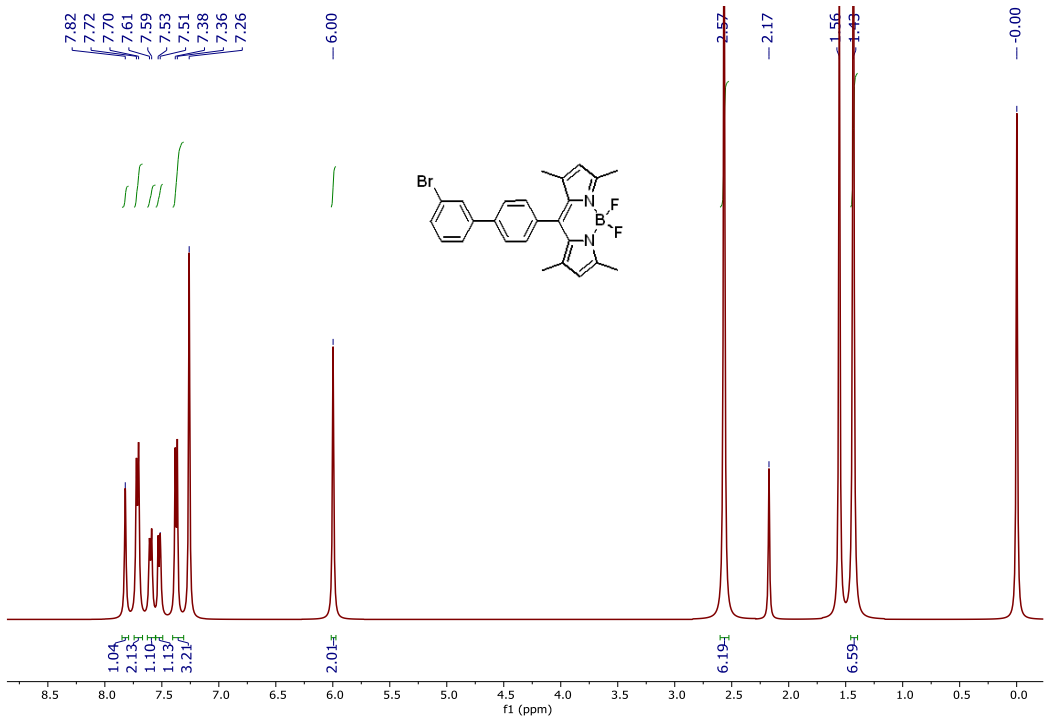

^{13}C NMR of *mp*-BODIPY:

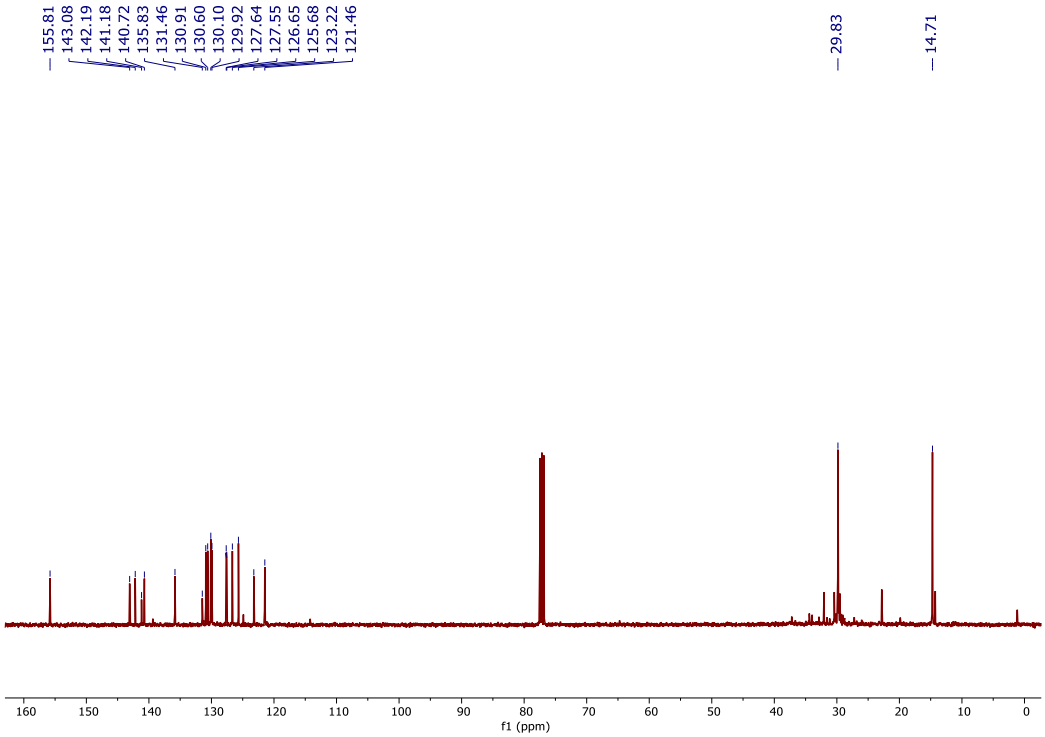

^{1}H NMR of *mm*-BODIPY:

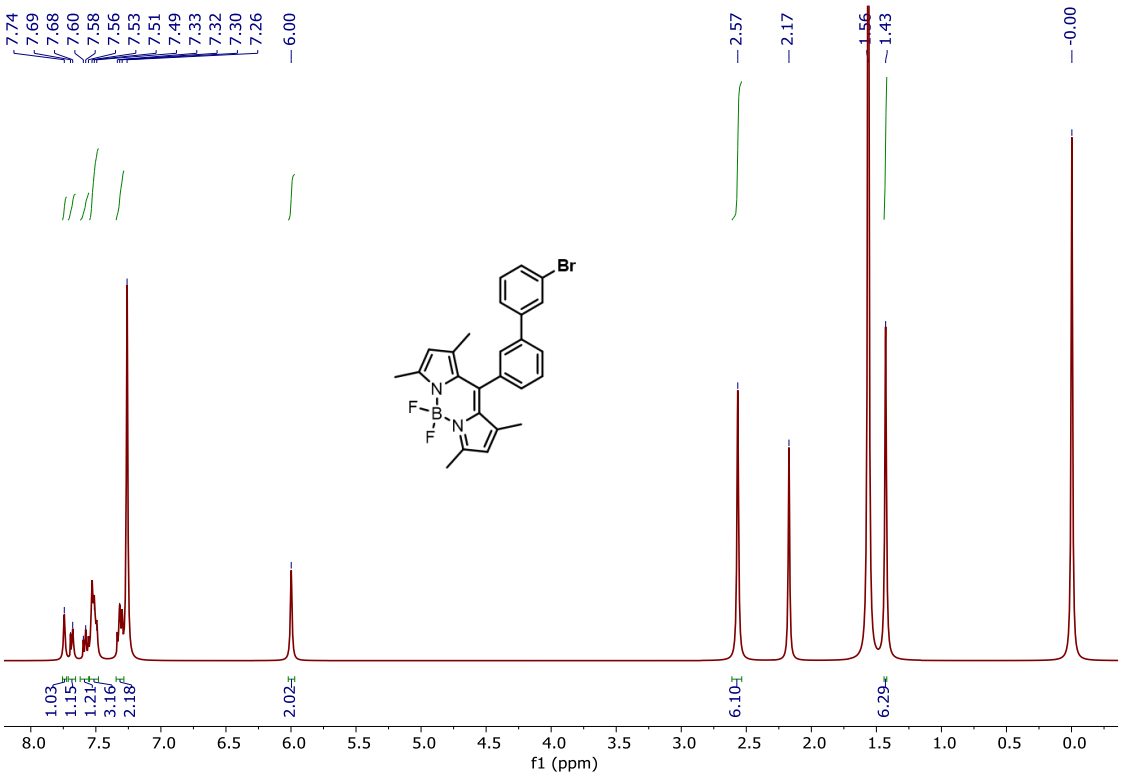

^{13}C NMR of *mm*-BODIPY:

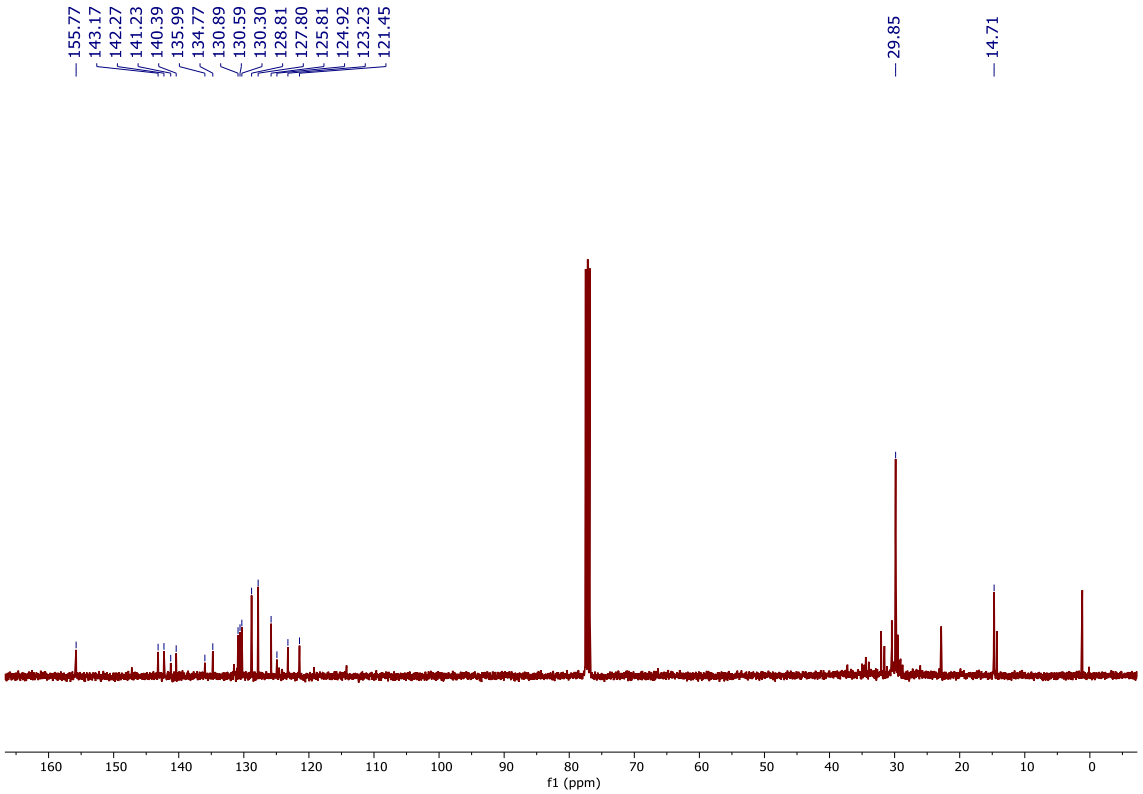

^{1}H NMR of Compound 4:

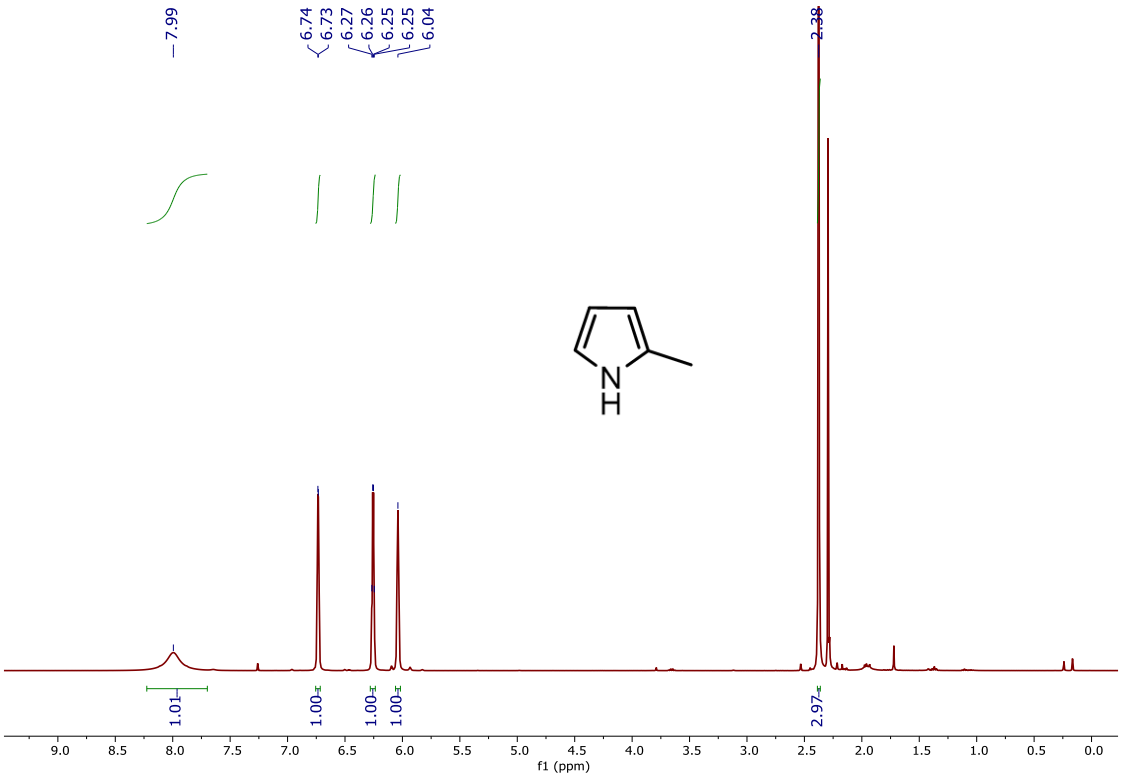

^{1}H NMR of T-BODIPY:

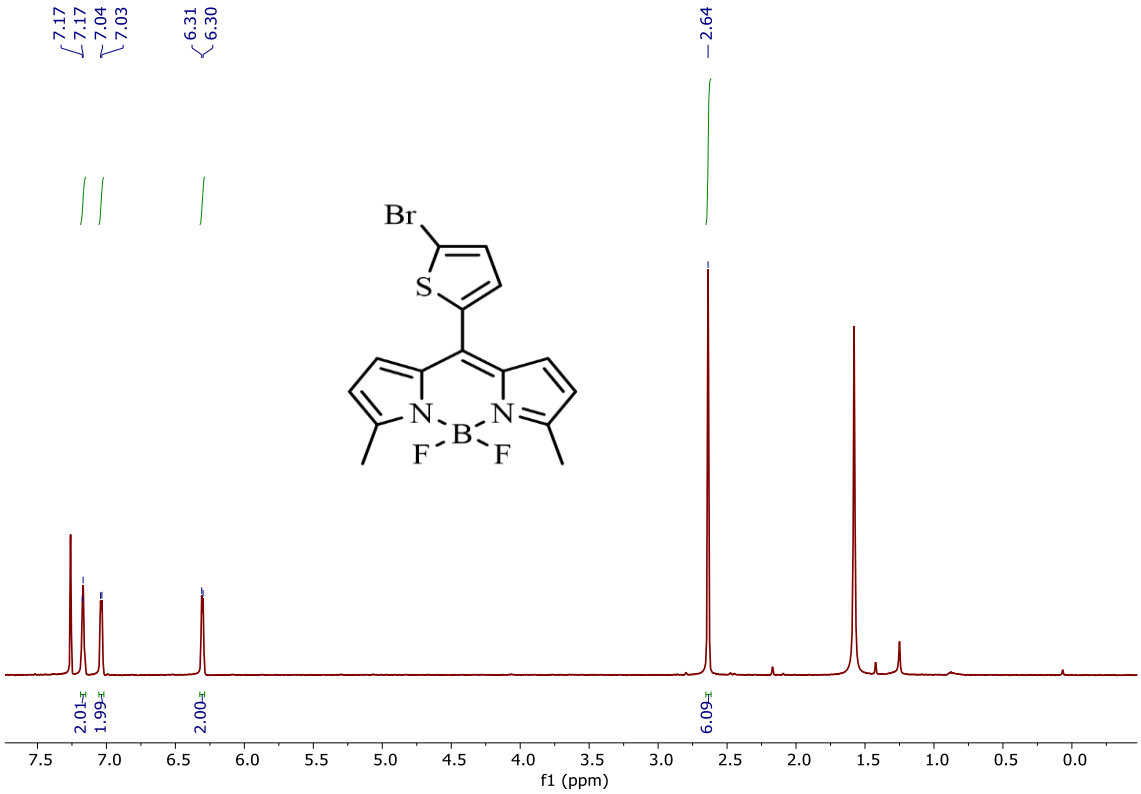

^{13}C NMR of T-BODIPY:

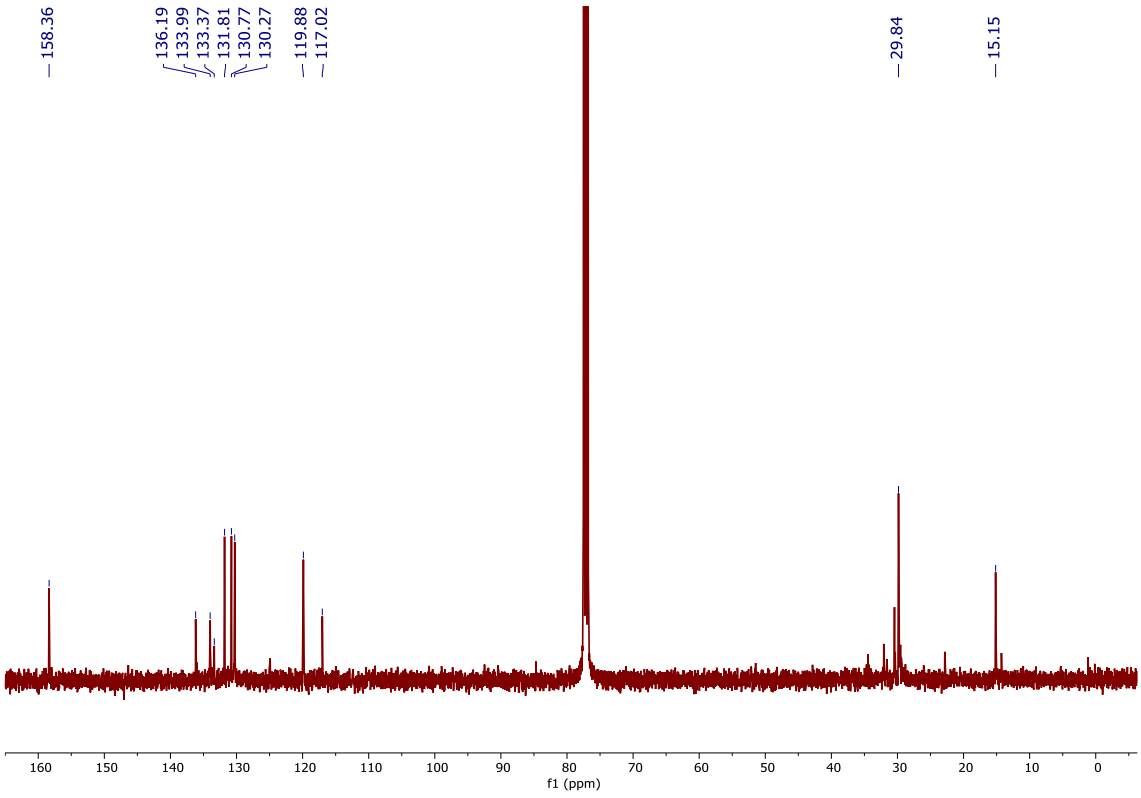

^{1}H NMR of T-ADA:

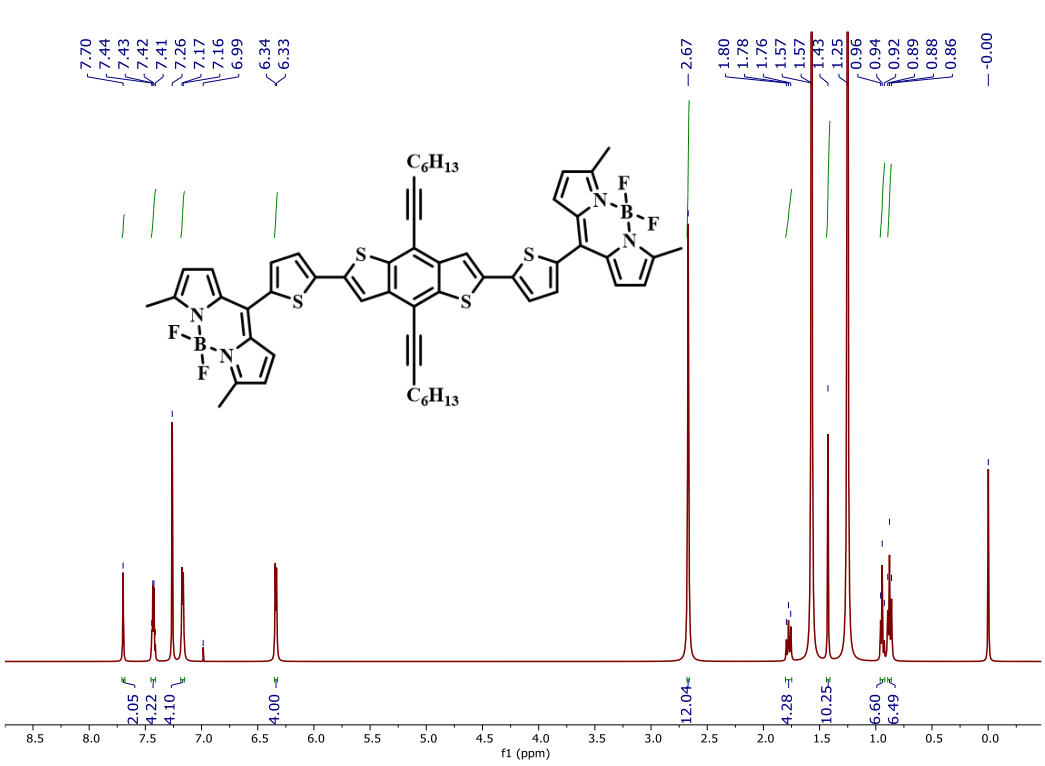

^{13}C NMR of T-ADA:

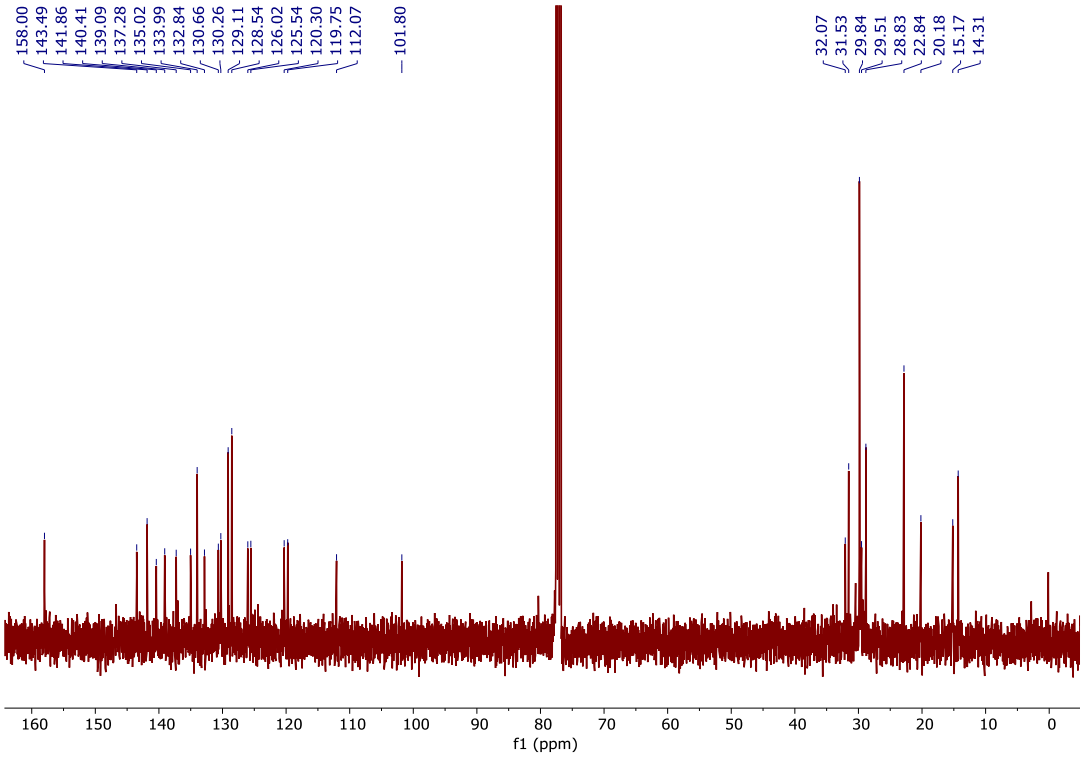

4. UV/Vis Absorption and Emission Spectra

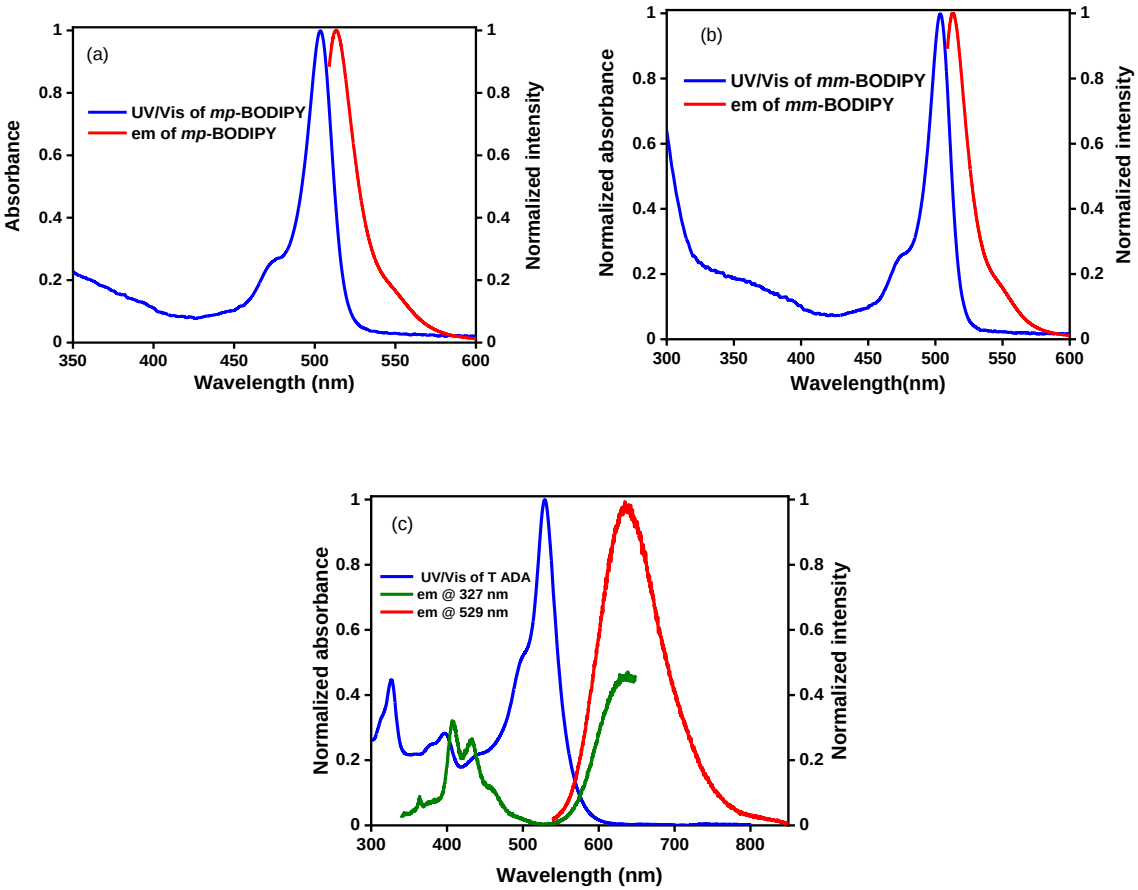

Figure S1. UV/Vis absorption and emission spectra of (a) ***mp*-BODIPY** (λ_{ex} = 504 nm)**,** (b) ***mm*-BODIPY** (λ_{ex} = 504 nm) and (c) **T-ADA** (λ_{ex} = 529 nm).

5. Fluorescence Quantum Yield

Fluorescence quantum yield was measured by using relative method using Rhodamine B (Φ_R = 0.5) in ethanol and 4',6-diamidino-2-phenylindole (DAPI, Φ_R = 0.58) in DMSO as reference dyes and using the following equation no. 1:[S8]

$$\mathbf{\Phi = \Phi_R\,(I/I_R)\,(A_R/A)\,(\lambda_{exR}/\lambda_{ex})\,(n^2/n^2_R)} \qquad \ldots.(1)$$

where Φ_R is the quantum yield of reference dye Rhodamine B in ethanol and DAPI in DMSO, I and I_R are integrated fluorescence intensities of compounds and reference dye respectively, A and A_R are the absorbance of the compounds and reference dye respectively, and n and n_R are the refractive indices of solvent(s) used for compounds and reference respectively. All the compounds ***pp*-BODIPY**, ***mp*-BODIPY**, ***mm*-BODIPY**, **T-BODIPY** and **T-ADA** were dissolved in $CHCl_3$ in three different concentrations ($c \sim 10^{-5}$-10^{-6} M) such that their absorbance was less than or equal to 0.1 and their absorption and fluorescence spectra were recorded (at

excitation wavelengths of 350 nm for all regioisomeric BODIPYs ***pp*-BODIPY**, ***mp*-BODIPY**, ***mm*-BODIPY** and 527 nm, 529 nm for **T-BODIPY** and **T-ADA** respectively). Absorbance and fluorescence spectra were recorded for three different concentrations of DAPI (excitation wavelength of ~ 360 nm) in DMSO and Rhodamine B (excitation wavelength of ~ 543 nm) in ethanol ($c \sim 10^{-5}$-10^{-6} M). Rhodamine B was employed as a reference dye for **T-BODIPY** and **T-ADA**, and DAPI was used for regioisomeric BODIPYs. Fluorescence quantum yields were then calculated using the above equation for each compound (Table S1).

Table S1: Relative quantum yields of ***pp*-BODIPY**, ***mp*-BODIPY**, ***mm*-BODIPY**, **T-BODIPY** and **T-ADA** using relative method and DAPI and Rhodamine B as a reference dye.

Compound	**Absorbance**			**Integrated Fluorescence Intensity**			**Quantum Yield** $\Phi=\Phi_R(I/I_R)(A_R/A)(\lambda_{exR}/\lambda_{ex})(n^2/n^2_R)$	
	1	**2**	**3**	**1**	**2**	**3**	Φ_i	Φ_{avg}
***pp*-BODIPY**	0.021	0.033	0.045	532.133	766.749	1032.316	0.696 0.731 0.675	0.70
***mp*-BODIPY**	0.024	0.044	0.052	552.470	960.946	1121.319	0.633 0.688 0.635	0.652
***mm*-BODIPY**	0.023	0.032	0.042	572.992	778.329	1094.169	0.685 0.766 0.767	0.739
T-BODIPY	0.045	0.057	0.068	75.567	89.267	103.753	0.134 0.140 0.141	0.138
T-ADA	0.038	0.058	0.071	91.192	121.353	151.747	0.193 0.186	0.191

							0.196
DAPI (DMSO)	0.0448	0.0707	0.0828	629.732	867.144	1086.253	0.58 (reported value)
Rhodamine B (ethanol)	0.033	0.065	0.105	234.7	418.247	655.36	0.5 (reported value)

6. Aggregation Induced Emission (AIE) of T-ADA

Generally, molecular rotors are weakly emissive in good solvents and become highly emissive in poor solvent due to and formation of aggregates and the resultant restricted intramolecular rotations. Aggregation induced emission (AIE) study was performed for **T-ADA** in a binary mixture of THF/water (v/v). As the water percentage was increased from 0% to 50% (v/v), the emission intensity was increased with a bathochromic shift of ~ 17 nm as shown in Figure S2. However, upon increasing the water percentage from 50% to 80%, the emission intensity increased by 2-fold with a slight hypsochromic shift of ~ 6 nm. Upon further increase in water percentage from 80% to onwards, the emission intensity decreased with a bathochromic shift of ~ 27 nm as shown in Figure S2. Figure S4b shows the changes in emission intensities and wavelengths with increase in water percentages from 0% to 99% in THF solution. UV/Vis absorption spectra of **T-ADA** were also measured in different THF and water mixtures (Figure S2c), where at higher percentages of water, the absorption band was bathochromically shifted with tailing in the long wavelength region indicative of the formation of nano-aggregates.

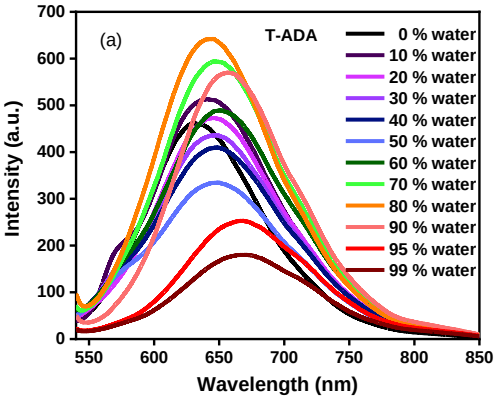

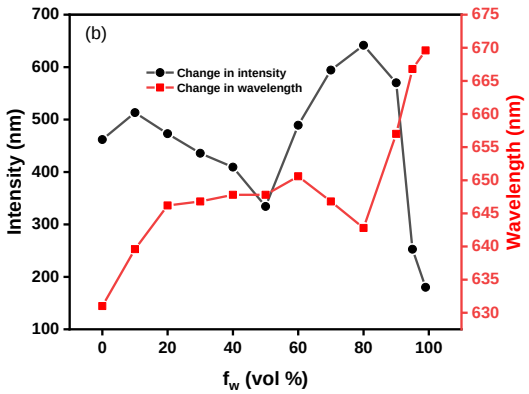

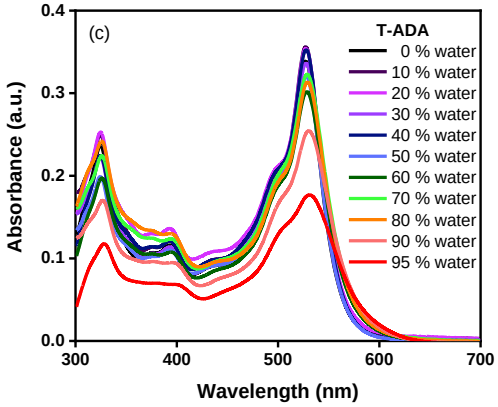

Figure S2. Emission of (a) **T-ADA** (λ_{ex} = 529 nm in different percentage of THF and water (*c* ~ 10^{-6} M) and (b) change in intensity and change in wavelength versus fraction of water (f_w) of **T-ADA**. UV/Vis absorption of (c) **T-ADA** in different percentages of THF and water.

7. Temperature-dependent Emission of T-ADA

Emission of molecular rotors is sensitive to various stimuli such as polarity, viscosity, and temperature. Hence, to study the effect of temperature on emission of **T-ADA**, temperature-dependent fluorescence measurements were performed in polar ($CHCl_3$) and non-polar (Tol) solvents from -5 °C up to the boiling point of solvent. In case of $CHCl_3$, upon increasing the temperature, the emission intensity of **T-ADA** decreased by ~ 4-fold with a hypsochromic shift of ~ 23 nm. Similarly, in case of Tol, the emission intensity of **T-ADA** decreased by ~ 2-fold with a hypsochromic shift of ~ 12 nm as shown in Figure S3. In both cases, the emission intensities decreased with increasing temperature due to the increase in non-radiative deactivation. The ratiometric temperature analysis of **T-ADA** was performed in $CHCl_3$ and Tol and fitted with linear function with goodness of fit R^2 values of 0.96 and 0.98 and the calculated internal sensitivities were 0.46 % $^oC^{-1}$ and 0.21% $^oC^{-1}$ respectively.

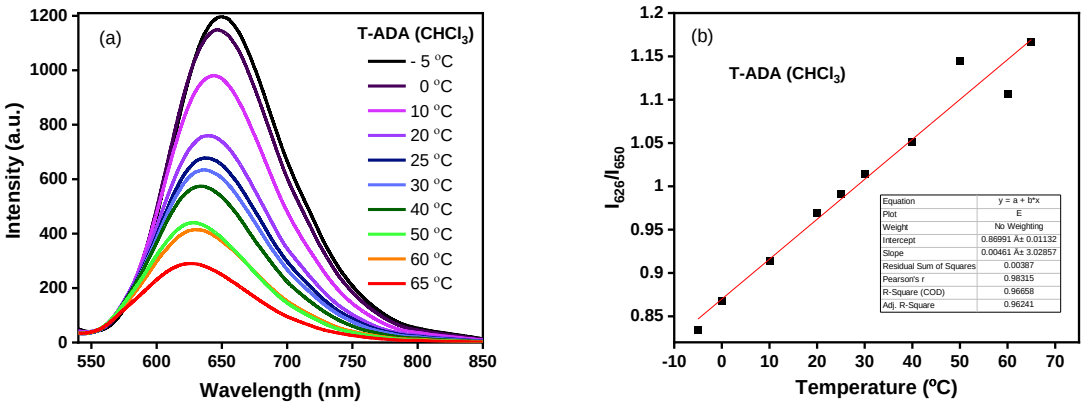

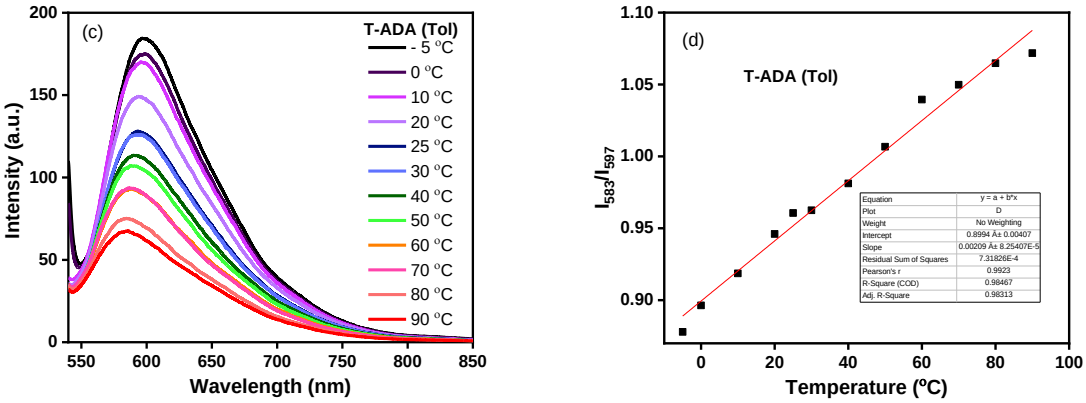

Figure S3. Temperature-dependent emission spectra of **T-ADA** (λ_{ex} = 529 nm) in (a) $CHCl_3$ and (c) Tol in 10^{-6} M concentration. Emission intensity ratio in (b) $CHCl_3$ and (d) Tol at different temperatures with best fit equations.

8. Cyclic Voltammetry:

Cyclic voltammetry (CV) measurements were performed for ***pp*-BODIPY**, ***mp*-BODIPY**, ***mm*-BODIPY**, **T-BODIPY** and **T-ADA** in dry DCM with 0.1 M tetrabutylammonium hexafluorophosphate as supporting electrolyte and Ag/AgCl as reference electrode to determine the HOMO and LUMO energy levels. Based on the first oxidation potential onset (E_{onset}^{ox}) and first reduction potential (E_{onset}^{red}), the HOMO and LUMO were calculated[S7] as using equation no. 2 and 3,

$$HOMO = -(E_{onset}^{ox} + 4.76)\ eV, \text{ and} \qquad \ldots.(2)$$

$$LUMO = -(E_{onset}^{red} + 4.76)\ eV \qquad \ldots.(3)$$

All the regioisomeric BODIPYs ***pp*-BODIPY**, ***mp*-BODIPY** and ***mm*-BODIPY** showed reversible peak upon applying potential + 2 V to -2 V as shown in Figure S4. While in case of **T-BODIPY** and **T-ADA**, a hump was seen while applying positive potential (0 to + 2 V) and a reversible peak was shown when applying negative potential (0 to - 2 V). The E_{onset}^{ox} and E_{onset}^{red} values as well as the calculated HOMO and LUMO values have been tabulated in Table S2. Accordingly, the calculated HOMO energies for ***pp*-BODIPY**, ***mp*-BODIPY**, ***mm*-BODIPY**, **T-BODIPY** and **T-ADA** are -5.93 eV, -5.95 eV, -5.88 eV, -6.01 eV and -5.74 eV respectively and LUMO energies are -4.06 eV, -4.11 eV, -4.22 eV, -3.98 eV and -4.12 eV respectively as shown in Table S2.

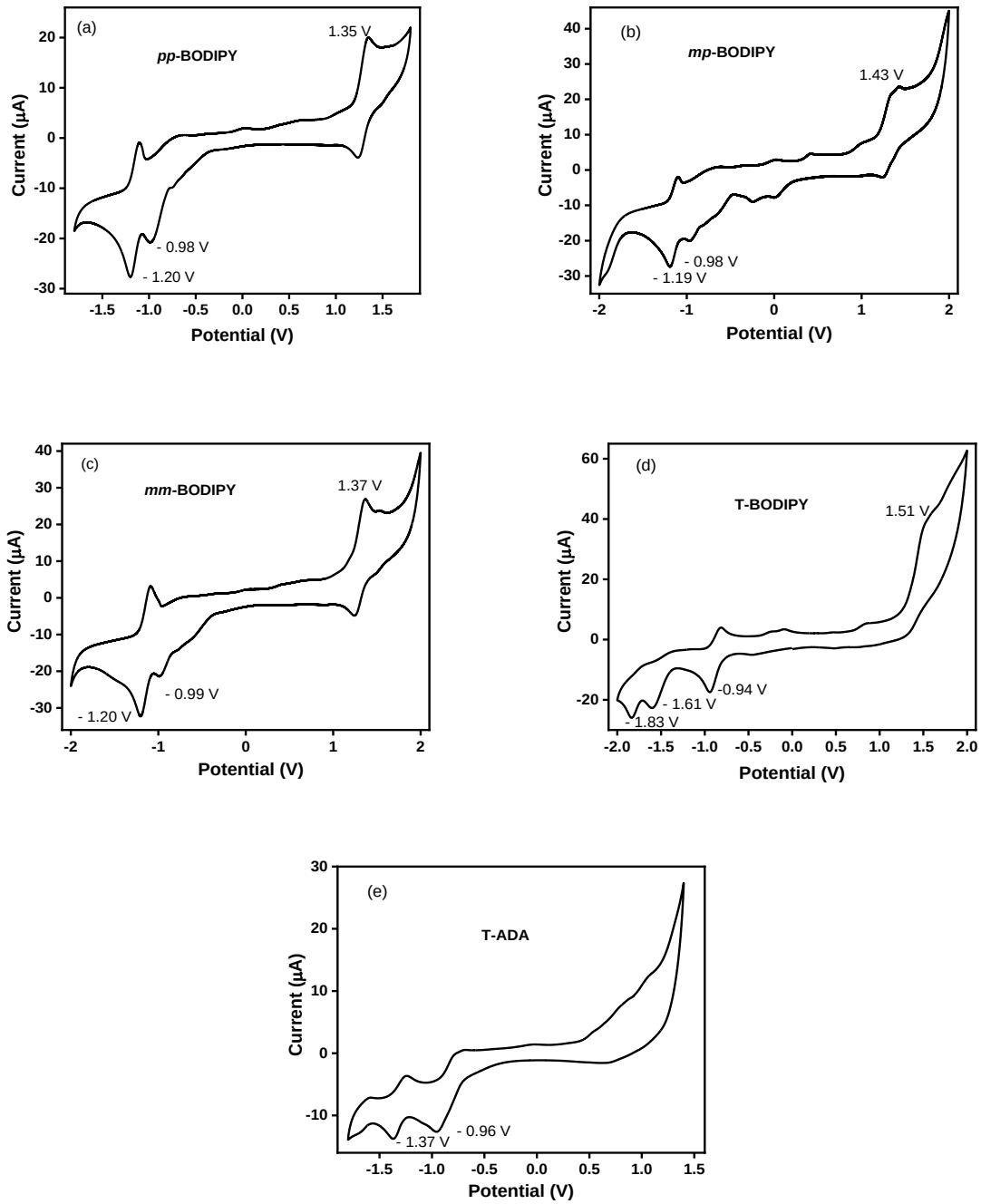

Figure S4. Cyclic voltammogram of (a) ***pp*-BODIPY**, (b) ***mp*-BODIPY**, (c) ***mm*-BODIPY** (d) **T-BODIPY** and (e) **T-ADA** in dry DCM with 0.1 M tetrabutylammonium hexafluorophosphate (TBAHPF) and potentials measured vs Ag/AgCl reference electrode.

Table S2. Redox and optical properties of ***pp*-BODIPY**, ***mp*-BODIPY**, ***mm*-BODIPY**, **T-BODIPY** and **T-ADA** based on cyclic voltammetry.

Compound	E_{ox}^{onset} (V)	HOMO (eV)	E_{red}^{onset} (V)	LUMO (eV)	E_g (eV)
***pp*-BODIPY**	1.17	-5.93	-0.70	-4.06	1.87
***mp*-BODIPY**	1.19	-5.95	-0.65	-4.11	1.84
***mm*-BODIPY**	1.12	-5.88	-0.54	-4.22	1.66

T-BODIPY	1.25	-6.01	-0.78	-3.98	2.03
T-ADA	0.98	-5.74	-0.64	-4.12	1.62

9. Spectroelectrochemistry

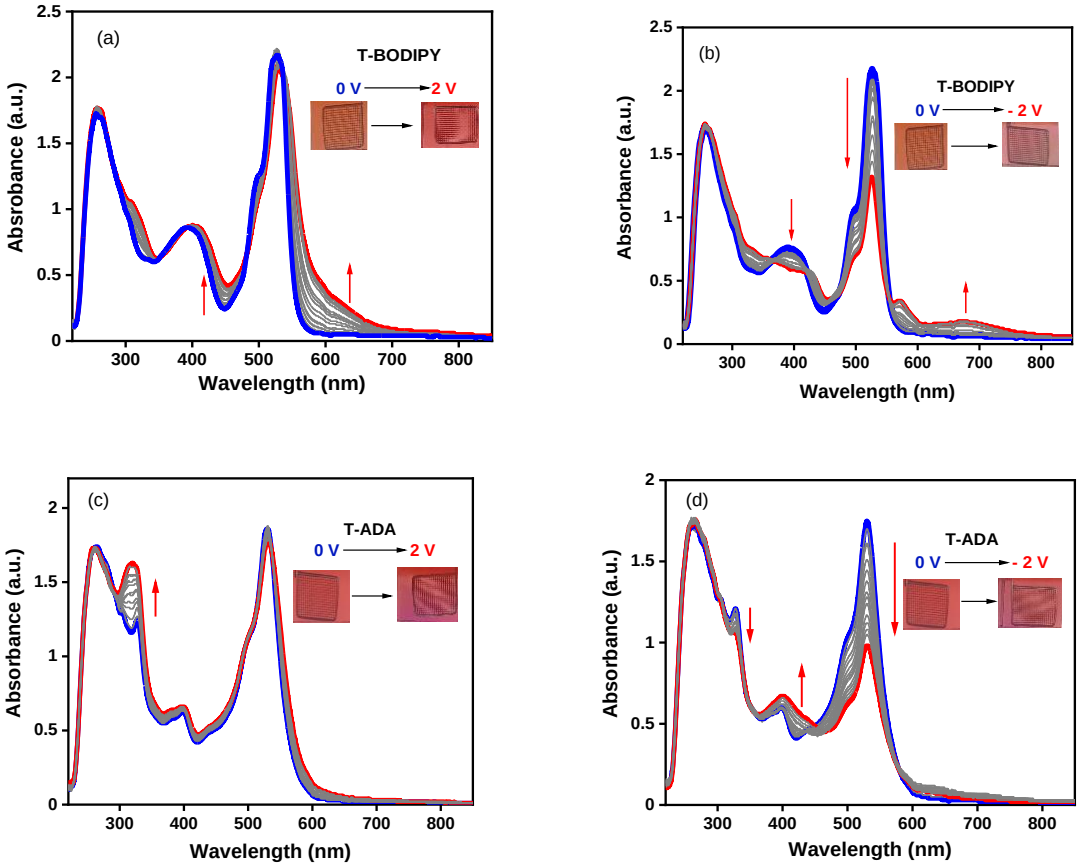

Figure S5. Spectroelectrochemical changes of (a, b) **T-BODIPY** and (c, d) **T-ADA**, upon applying positive potential (0 to 2 V) and negative potential (0 to -2 V) in DCM upto 40 cycles. Figure inset showed the change of colour of solution after applying potential.

10. DFT Calculations

Density functional theory (DFT) calculations were performed for all molecules in the ground state using the Gaussian 09 package[S1] at the B3LYP/6-31G(d,p) level to calculate the HOMO and LUMO energy levels in geometry optimized structures. The DFT calculated energy levels are presented in the Figure S6 and S7 and Table S3. In case of regioisomeric BODIPYs ***pp*-BODIPY**, ***mp*-BODIPY** and ***mm*-BODIPY**, both HOMO and LUMO was completely localized on BODIPY part and LUMO +1 was localized on biphenyl part as shown in Figure S6. While in case of **T-BODIPY** HOMO was localized on BODIPY part and LUMO was

localized on the whole molecule. In case of **T-ADA**, HOMO was completely localized on BDT part and LUMO was localized on BODIPY and a small part on BDT while LUMO +1 was completely localized on BODIPY part showed possibility of charge transfer from HOMO to LUMO and HOMO to LUMO +1 as shown in Figure S7.

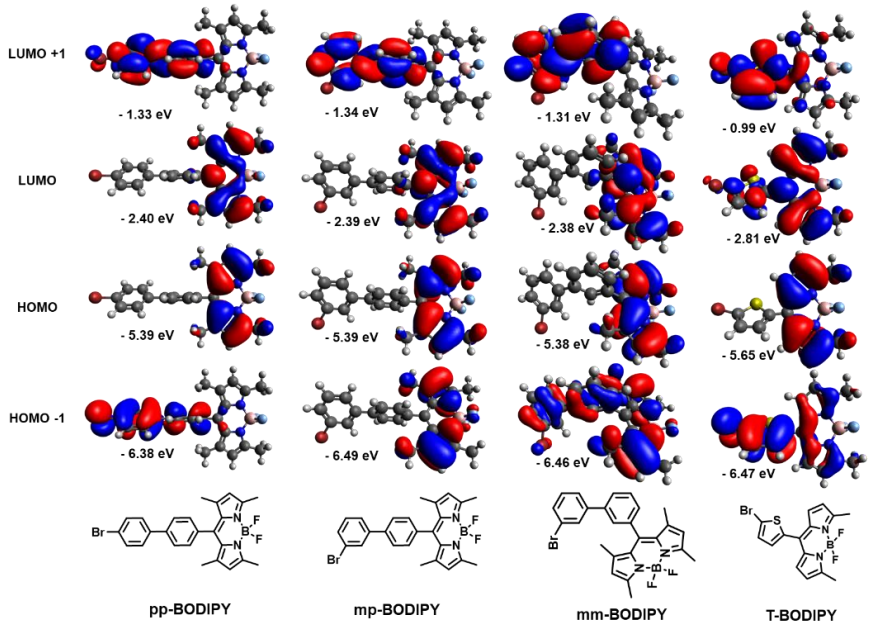

Figure S6. FMO energy levels of compounds ***pp*-BODIPY**, ***mp*-BODIPY, *mm*-BODIPY** and **T-BODIPY** calculated using B3LYP/6-31G(d,p).

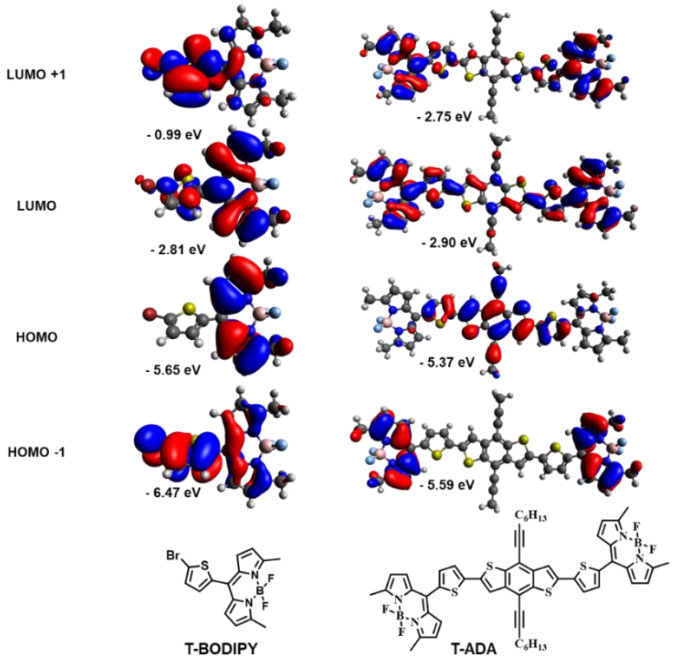

Figure S7. FMO energy levels of compounds **T-BODIPY** and **T-ADA** calculated using B3LYP/6-31G(d,p).

Table S3. FMO energy levels of compounds ***pp*-BODIPY**, ***mp*-BODIPY**, ***mm*-BODIPY**, **T-BODIPY** and **T-ADA** calculated by B3LYP/6-31G(d,p).

Compound	HOMO-1 (eV)	HOMO (eV)	LUMO (eV)	LUMO+1 (eV)	ΔE (eV)	Dihedral angle (°)
***pp*-BODIPY**	-6.38	-5.39	-2.40	-1.33	2.99	89.5
***mp*-BODIPY**	-6.49	-5.39	-2.39	-1.34	3.00	90.4
***mm*-BODIPY**	-6.46	-5.38	-2.38	-1.31	3.00	91.8
T-BODIPY	-6.47	-5.65	-2.81	-0.99	2.84	48.9
T-ADA	-5.59	-5.37	-2.90	-2.75	2.47	47.5

Table S4. Singlet and triplet energies of various states of **T-BODIPY** and **T-ADA** calculated using TD-DFT calculations.

Compound	S_1 (eV)	S_2 (eV)	T_1 (eV)	T_2 (eV)	T_3 (eV)	T_4 (eV)	ΔE_{ST} (eV)
T-BODIPY	2.73	3.04	1.47	2.44	2.75	2.98	0.02 (S_1 & T_3)
T-ADA	2.06	2.23	1.46	1.46	1.59	1.96	0.10 (S_1 & T_4)

Table S5. Singlet (S_1) and triplet energy (T_4) values of **T-ADA** in $CHCl_3$ and heptane calculated using TD-DFT using PCM.

Compound	S_1 (eV)	T_4 (eV)
Heptane	2.73	3.04
$CHCl_3$	2.06	2.23

Table S6. Calculated dipole moments and oscillator strengths of different singlet states of **T-BODIPY** and **T-ADA** by TD-DFT calculations.

Singlet states	T-BODIPY		T-ADA	
	Dipole moment	Oscillator strength	Dipole moment	Oscillator strength
S_1	9.76	0.49	16.66	1.09
S_2	7.45	0.32	16.66	0.003
S_3	3.22	0.06	3.50	0.059
S_4	2.32	0.03	6.46	0.20

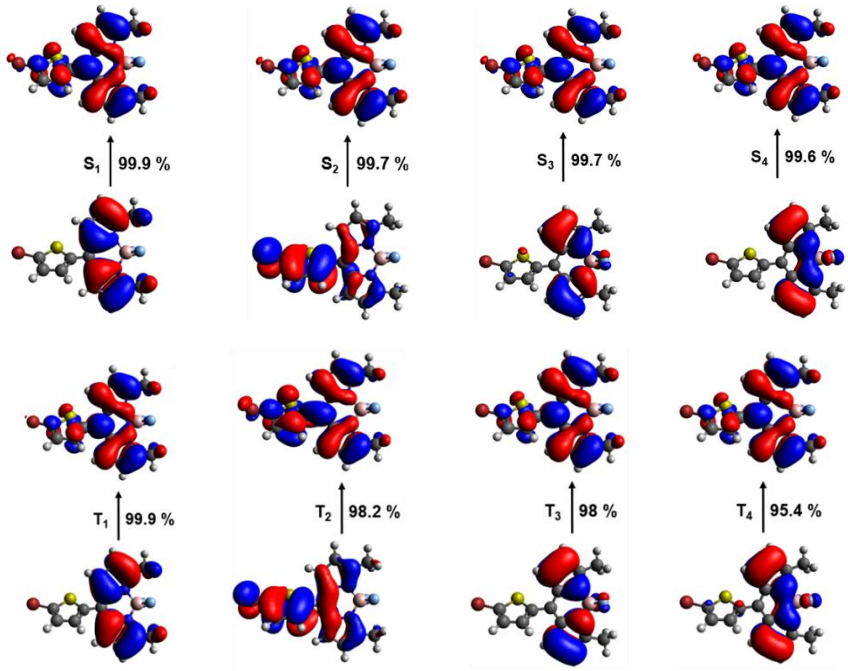

Figure S8. The natural transitions orbitals (NTOs) for singlet and triplet states of **T-BODIPY** calculated using TD-DFT.

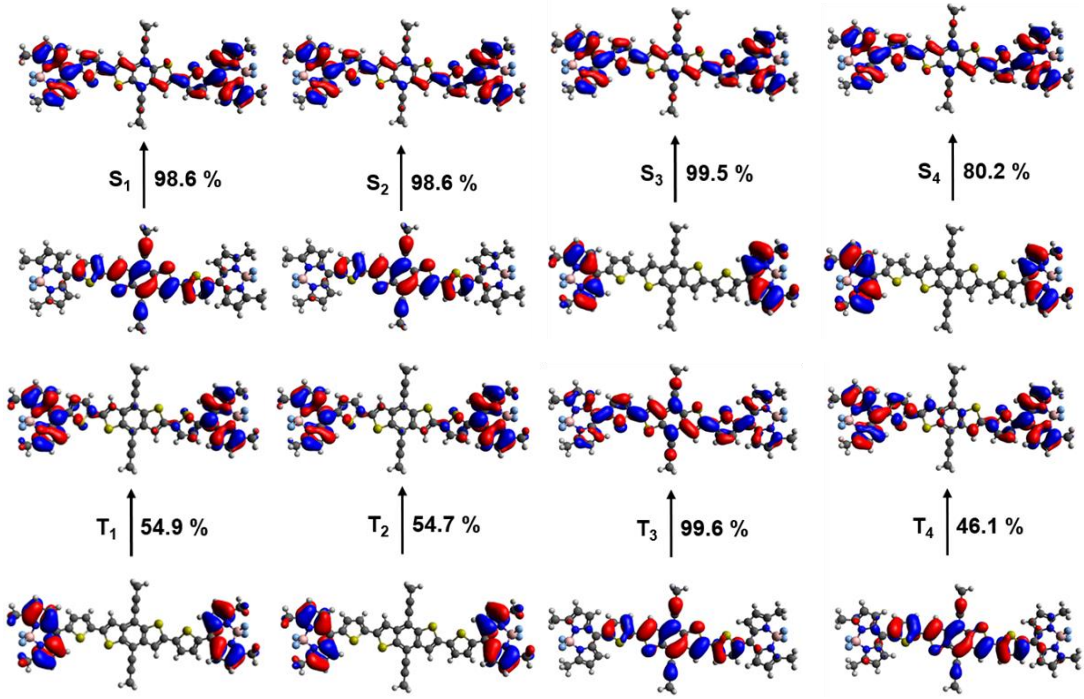

Figure S9. The natural transitions orbitals for singlet and triplet states of **T-ADA** calculated using TD-DFT.

Frontier molecular orbital (FMO) composition analysis was conducted for ***pp*-BODIPY**, ***mp*-BODIPY**, ***mm*-BODIPY**, **T-BODIPY** and **T-ADA** and it was found that in case of regioisomeric BODIPYs (***pp*-BODIPY**, ***mp*-BODIPY**, ***mm*-BODIPY**), the HOMO was composed of 0% contribution from biphenyl part and 100% contribution from BODIPY part.

The LUMO was composed of 98% contribution from BODIPY part and 2% from biphenyl part indicating no possibility of charge transfer from biphenyl to BODIPY. In case of **T-BODIPY**, the HOMO was composed of 1% contribution from thiophene part and 99% contribution from BODIPY part, while LUMO was composed of 86% contribution from BODIPY part and 2% from thiophene part, suggesting a lower possibility of charge transfer from thiophene to BODIPY part. In case of **T-ADA**, the HOMO was composed of 95% contribution from BDT part and 5% contribution from BODIPY part, while LUMO was composed of 66% contribution from BODIPY part and 34% from BDT part, indicating charge transfer character from BDT to BODIPY part as shown in Table S7.

Table S7. FMO composition analysis for ***pp*-BODIPY**, ***mp*-BODIPY**, ***mm*-BODIPY**, **T-BODIPY** and **T-ADA** based on DFT calculations.

Compound	Orbital No.	MO	Energy (eV)	Contribution from donor (%)	Contribution from acceptor (%)
***pp*-BODIPY**	124	LUMO+1	-1.33	98	2
	123	LUMO	-2.40	2	98
	122	HOMO	-5.39	0	100
	121	HOMO-1	-6.38	98	2
***mp*-BODIPY**	159	LUMO+1	-1.34	98	2
	158	LUMO	-2.39	2	98
	157	HOMO	-5.39	0	100
	156	HOMO-1	-6.49	1	99
mm-BODIPY	279	LUMO+1	-1.31	98	2
	278	LUMO	-2.38	2	98
	277	HOMO	-5.38	0	100
	276	HOMO-1	-6.46	19	81
T-BODIPY	279	LUMO+1	-0.99	88	12
	278	LUMO	-2.81	14	86
	277	HOMO	-5.65	1	99
	276	HOMO-1	-5.37	80	20
T-ADA	279	LUMO+1	-2.75	18	82
	278	LUMO	-2.90	34	66
	277	HOMO	-5.37	95	5
	276	HOMO-1	-5.59	1	99

Gibbs free energy of charge separation calculation:

The Gibbs free energy of charge separation (ΔG_{cs}^{0}) for **T-ADA** were calculated to assess the feasibility of charge transfer using Rehm–Weller equations Eq. no. 4[S9-S10]:

$$-\Delta G^0_{cs} = -E_{00} - \Delta G_{CR} \quad \ldots(4)$$

where, ΔG_{CR} is the Gibbs free energy of charge recombination and calculated by given equation no. 5:

$$\Delta G^0{}_{CR} = e[E_{ox}(D) - E_{red}(A)] + \Delta G_S \quad \ldots.(5)$$

where, e is the electronic charge, E_{ox} (D) is the first oxidation potential of donor and E_{red} (A) is the first reduction potential of acceptor, E_{00} is the energy of the $S_0 \rightarrow S_1$ transition (calculated by taking the intersection point of normalized absorption and emission spectra).

The static Coulombic energy ΔG_S is given by the following equation Eq. no. 6:

$$\Delta G_S = \frac{e^2}{4\pi\varepsilon_S\,\varepsilon_0\,Rcc} - \frac{e^2}{8\pi\varepsilon_0}\left(\frac{1}{R_D} + \frac{1}{R_A}\right)\left(\frac{1}{\varepsilon_{ref}} - \frac{1}{\varepsilon_S}\right) \quad \ldots.(6)$$

where, ε_S is the dielectric constant of the solvent, ε_{Ref} is the dielectric constant of the solvent used for experiment, ε_0 is the permittivity of free space. R_D and R_A refer to the effective radii of donor and acceptor and were estimated from the Connolly molecular surfaces volume of the respective moieties calculated with MM2 using the Chem3D Pro software[S11] and R_{cc} is the distance between the centers of the donor and acceptor.

Standard oxidation potential of donor in DCM; $E^0_{D+./D}$ = +1.34 V

Standard reduction potential of acceptor in DCM; $E^0_{A/A-.}$ = -0.87 V

Average radii of donor; R_A= 4.84 Å

Average radii of acceptor; R_A= 4.89 Å

Center to center distance of donor and acceptor segment, R_{cc} = 10.48 Å

Using the above relations, the driving force for both photoinduced charge separation and charge recombination processes between donor and acceptor were calculated and the observed values were – 0.30 eV and – 2.54 eV in Tol respectively. The negative values of $\Delta G^0{}_{CS}$ and $\Delta G^0{}_{CR}$ indicate that both photoinduced forward and backward electron transfer processes are exergonic and thermodynamically feasible for **T-ADA**.

11. Fluorescence lifetime

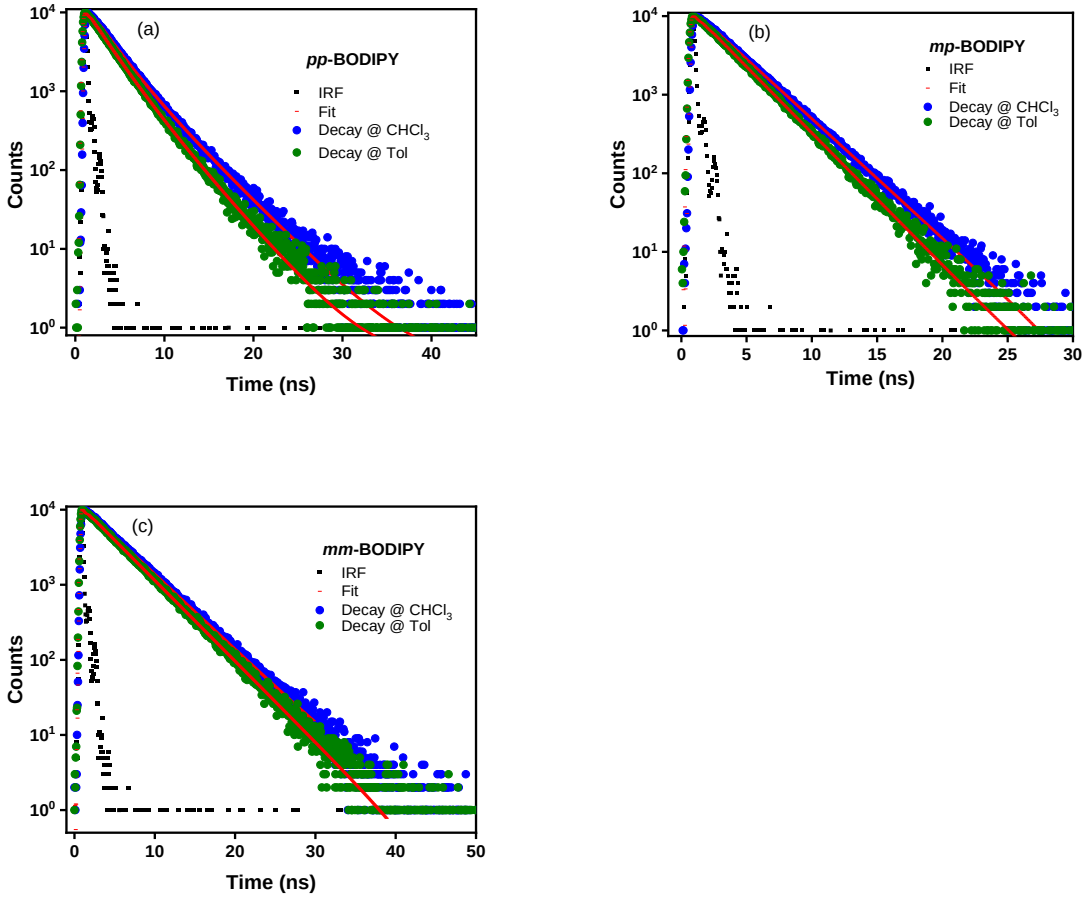

Figure S10. Fluorescence lifetime decay collected using a single photon counting technique in $CHCl_3$ and Tol of (a) ***pp*-BODIPY**, (b) ***mp*-BODIPY** and (c) ***mm*-BODIPY**.

Table S8. Fluorescence lifetime analyses of ***pp*-BODIPY**, ***mp*-BODIPY**, ***mm*-BODIPY**, **T-BODIPY** and **T-ADA** at different emission wavelengths.

Compound (λ_{ex} = 375 nm)	**Solvent**	λ_{em} **(nm)**	$\tau_1(\alpha_1)$ **(ns)**	$\tau_2(\alpha_2)$ **(ns)**	τ_{avg} **(ns)**	χ^2
	$CHCl_3$	513	3.1	-	--	1.18
***pp*-BODIPY**	Tol	513	2.8	-	-	1.14
	$CHCl_3$	513	2.9	-	-	1.12
***mp*-BODIPY**	Tol	513	2.7	-	-	1.13

	$CHCl_3$	513	4.4	-	-	1.05
***mm*-BDP**	Tol	513	4.1	-	-	1.03
	$CHCl_3$	554	0.35 (0.98)	4.74 (0.02)	0.44	1.19
T-BDP	Tol	554	0.38 (0.98)	4.39 (0.02)	0.45	0.98
T-ADA	$CHCl_3$	650	0.44 (0.94)	1.17 (0.06)	0.45	1.10

12. Singlet Oxygen ($^1O_2$) Quantum Yields

Singlet oxygen quantum yield (Φ_Δ) was determined by monitoring the photooxidation of 1,3-diphenylisobenzofuran (DPBF) as shown in Figure S11-S14 and Table S9. Diphenylisobenzofuran (DPBF) is a well-known $^1O_2$ scavenger and rapidly gives colourless oxidized product. It absorbs in visible region (~ 410 nm) and due to scavenges $^1O_2$, the absorbance decreases with time. Singlet oxygen quantum yield were calculated at low concentration (5 μM of dyes and 50 μM of DPBF) to minimize the possibility of quenching of $^1O_2$ by dyes. The quantum yields were calculated by relative method using Eosin Y (singlet oxygen quantum yield ~ 60%) as reference dye and using the following equations[S12] Eq. no. 7:

$$\Phi_\Delta^{dye} = \Phi_\Delta^{ref} (m^{dye}.F^{ref}/m^{ref}.F^{dye}) \qquad \ldots(7)$$

Where Φ_Δ^{ref} is the singlet oxygen quantum yield of Eosin Y, m is the slope of a plot of difference in change in absorbance of DPBF (~ 410 nm) with the irradiation time and F is the absorption correction factor given by $F = 1 - 10^{-OD}$ (optical density at irradiation wavelength). For the calculation of Φ_Δ, the solution of dye (c ~ 5 μM) and DPBF (*c* ~ 50 μM) in THF were taken in 20 mL round bottomed flask with a stir bar. The mixture was stirred for 2 minutes in dark and then sample were taken out for zero reading. Then the solution mixture was irradiated with monochromatic light source using KiloArc 1000W Xenon UV lamp at specific wavelength and aliquots were taken out at every interval of 1 min. The irradiation wavelength for ***pp*-BODIPY**, ***mp*-BODIPY**, ***mm*-BODIPY**, **T-BODIPY, T-ADA** and Eosin Y were 500 nm, 500 nm, 500 nm, 524 nm, 526 nm and 542 nm respectively.

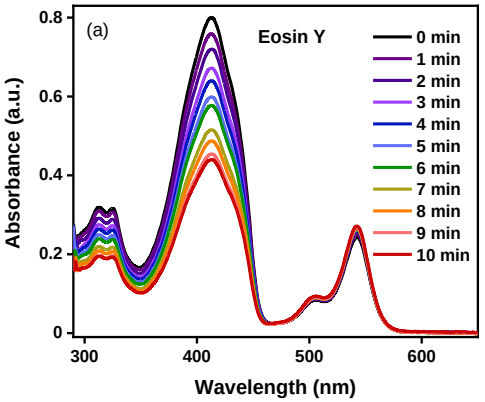
(a)
Eosin Y
0 min
1 min
2 min
3 min
4 min
5 min
6 min
7 min
8 min
9 min
10 min
Absorbance (a.u.)
Wavelength (nm)

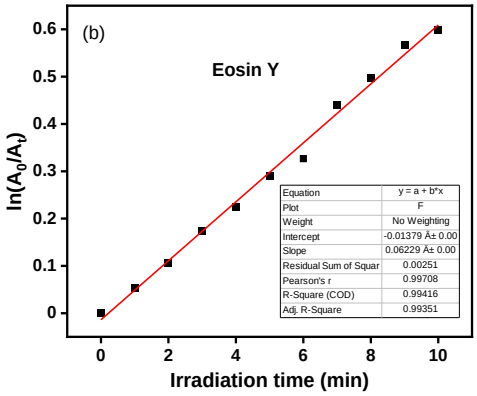
(b)
Eosin Y
ln(A0/At)
Irradiation time (min)
Equation y = a + b*x
Plot F
Weight No Weighting
Intercept -0.01379 ± 0.00
Slope 0.06229 ± 0.00
Residual Sum of Squar 0.00251
Pearson's r 0.99708
R-Square (COD) 0.99416
Adj. R-Square 0.99351

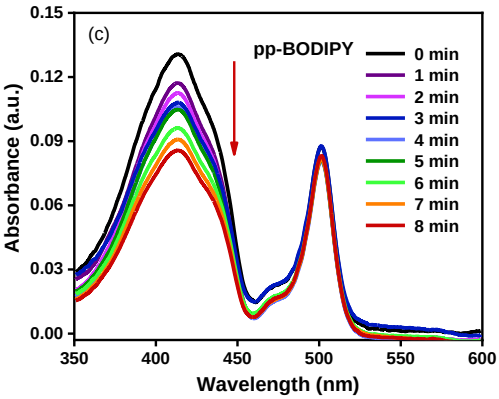
(c)
pp-BODIPY
0 min
1 min
2 min
3 min
4 min
5 min
6 min
7 min
8 min
Absorbance (a.u.)
Wavelength (nm)

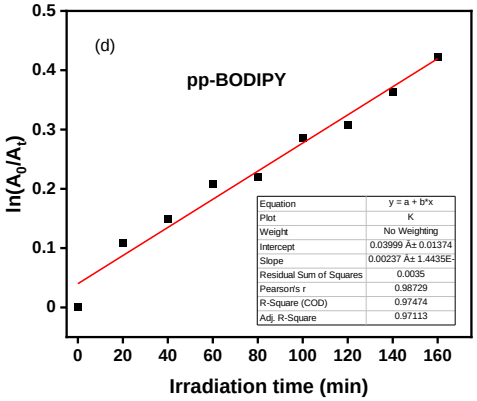
(d)
pp-BODIPY
ln(A0/At)
Irradiation time (min)
Equation y = a + b*x
Plot K
Weight No Weighting
Intercept 0.03999 ± 0.01374
Slope 0.00237 ± 1.4435E-
Residual Sum of Squares 0.0035
Pearson's r 0.98729
R-Square (COD) 0.97474
Adj. R-Square 0.97113

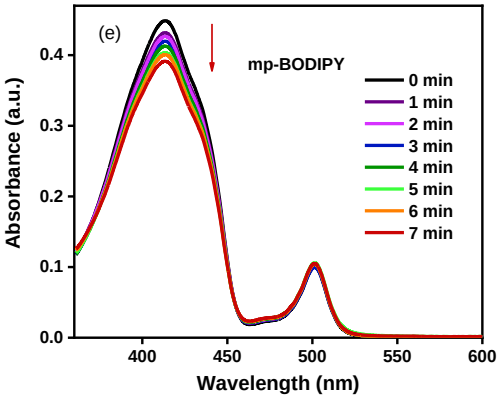
(e)
mp-BODIPY
0 min
1 min
2 min
3 min
4 min
5 min
6 min
7 min
Absorbance (a.u.)
Wavelength (nm)

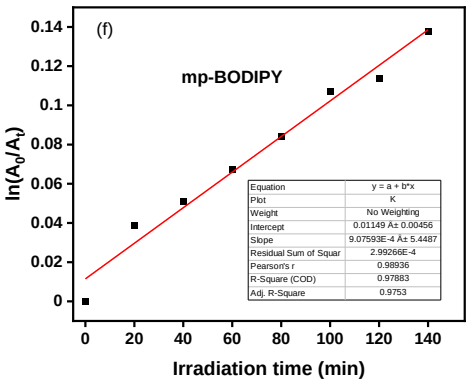
(f)
mp-BODIPY
ln(A0/At)
Irradiation time (min)
Equation y = a + b*x
Plot K
Weight No Weighting
Intercept 0.01149 ± 0.00456
Slope 9.07593E-4 ± 5.4487
Residual Sum of Squar 2.99266E-4
Pearson's r 0.98936
R-Square (COD) 0.97883
Adj. R-Square 0.9753

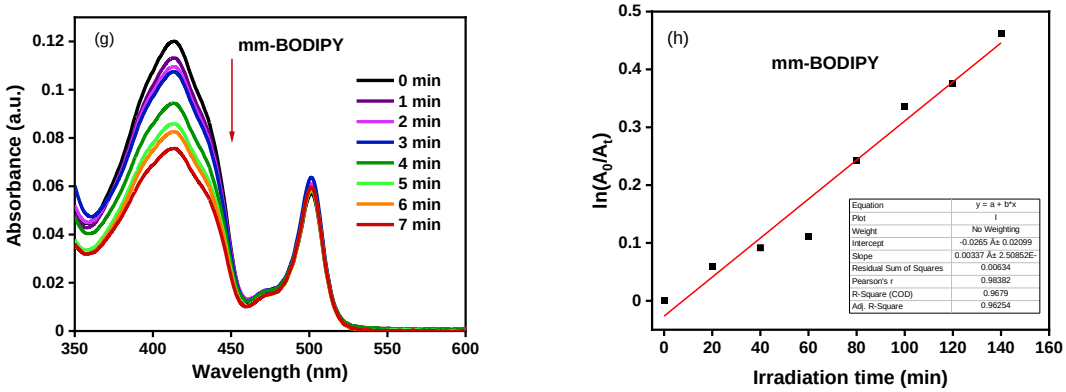

Figure S11. Changes in absorbance spectrum of DPBF upon irradiation in presence of (a) Eosin Y, (c) ***pp*-BODIPY**, (e) ***mp*-BODIPY**, (g) ***mm*-BODIPY** in different interval of time and plot of changes in absorption at A_0 and A_t with respect to irradiation time of (b) Eosin Y, (d) ***pp*-BODIPY**, (f) ***mp*-BODIPY**, (h) ***mm*-BODIPY** in THF. A_0- absorbance at time = 0 min and A_t- absorbance at time = t.

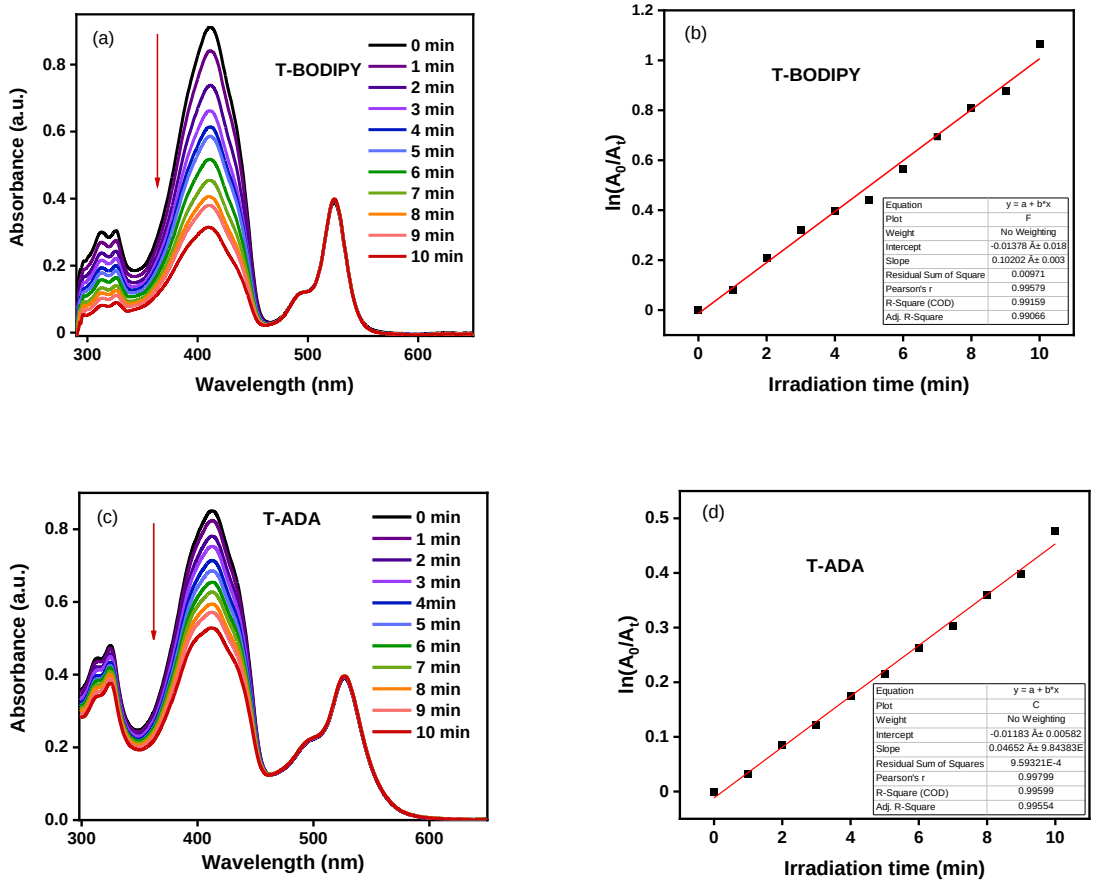

Figure S12. Changes in absorbance spectrum of DPBF upon irradiation in presence of (a) **T-BODIPY**, (c) **T-ADA**, in different interval of time and plot of change in absorption at A_0 and A_t with respect to irradiation time of (b) **T-BODIPY**, (d) **T-ADA** in THF. A_0 - absorbance at time = 0 min and A_t- absorbance at time = t.

Table S9. Relative singlet oxygen quantum yields of ***pp*-BODIPY**, ***mp*-BODIPY**, ***mm*-BODIPY**, **T-BODIPY** and **T-ADA** using relative method and Eosin Y as a reference dye.

Compounds	*pp*-BODIPY	*mp*-BODIPY	*mm*-BODIPY	T-BODIPY	T-ADA
Singlet oxygen quantum yield (THF) (%)	5.7	1.9	12.2	77	35
Singlet oxygen quantum yield (MeOH) (%)	0.4	0.3	0.5	17	6.4

Singlet QY in MeOH

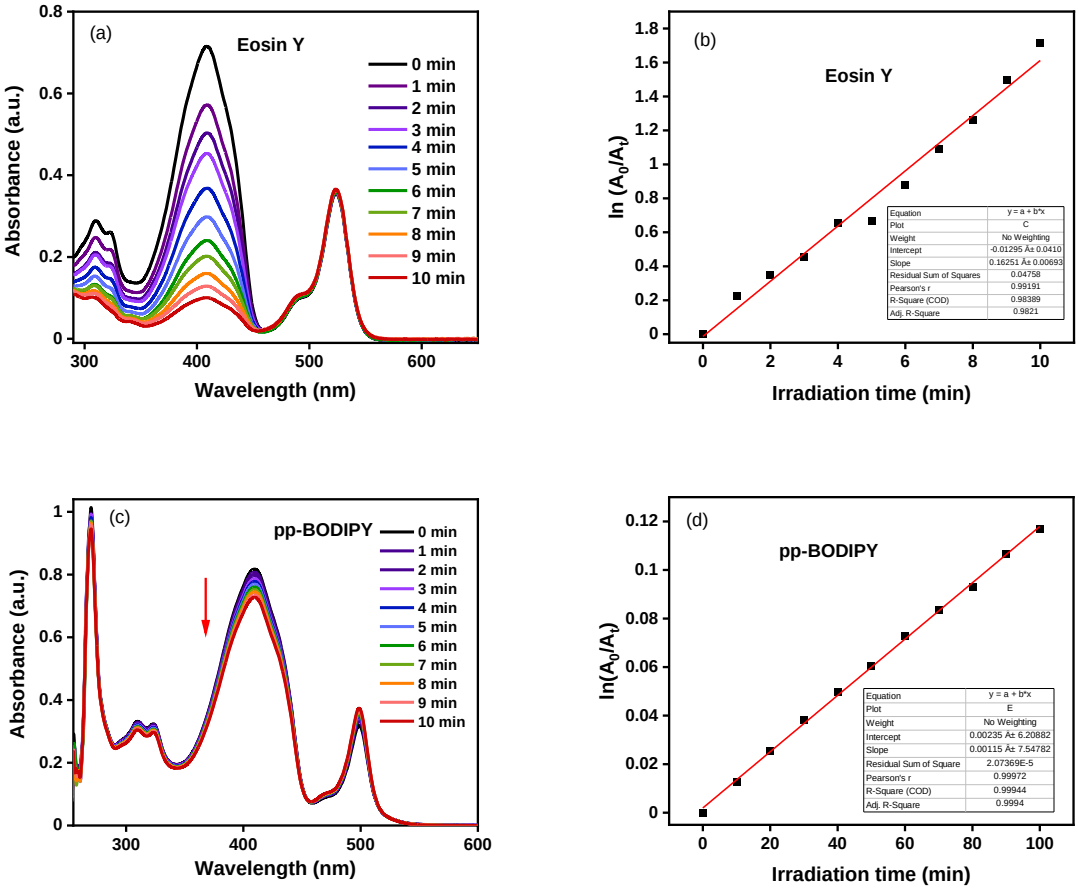

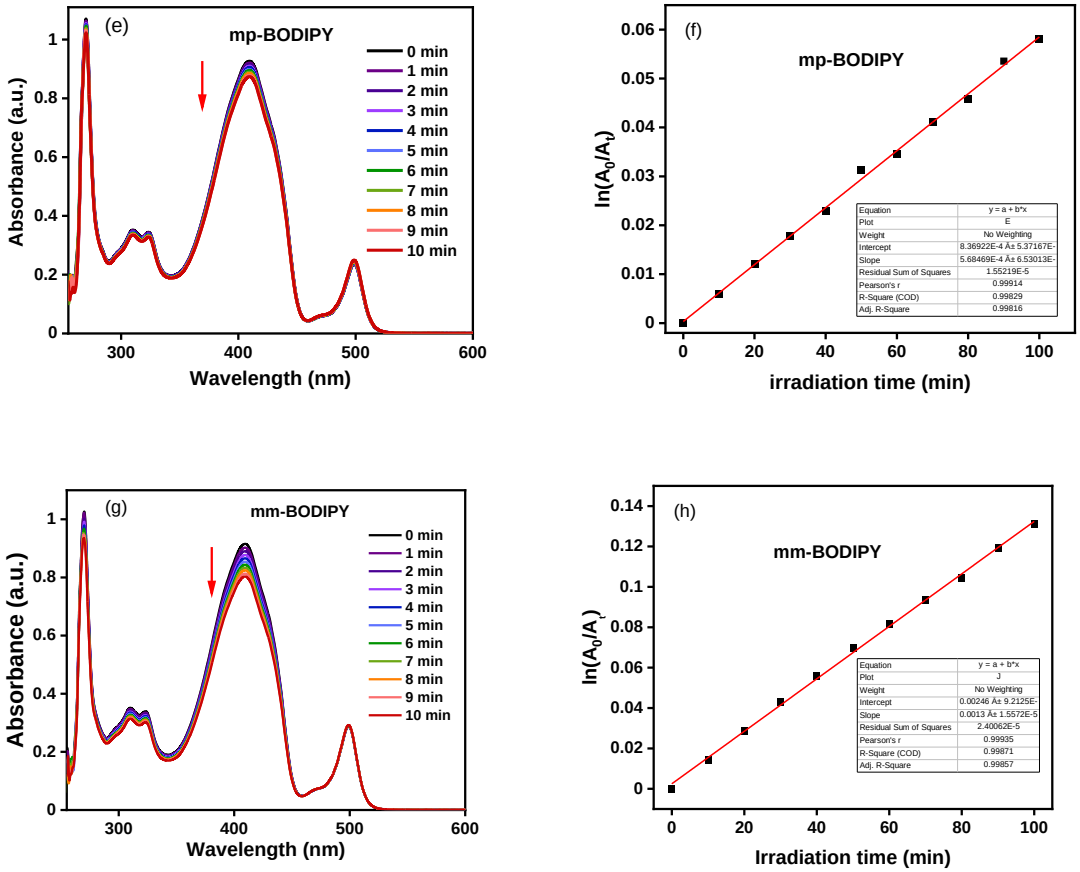

Figure S13. Changes in absorbance spectrum of DPBF upon irradiation in presence of (a) Eosin Y, (c) ***pp*-BODIPY**, (e) ***mp*-BODIPY**, (g) ***mm*-BODIPY** in different interval of time and plot of changes in absorption at A_0 and A_t with respect to irradiation time of (b) Eosin Y, (d) ***pp*-BODIPY**, (f) ***mp*-BODIPY**, (h) ***mm*-BODIPY** in MeOH. A_0- absorbance at time = 0 min and A_t- absorbance at time = t.

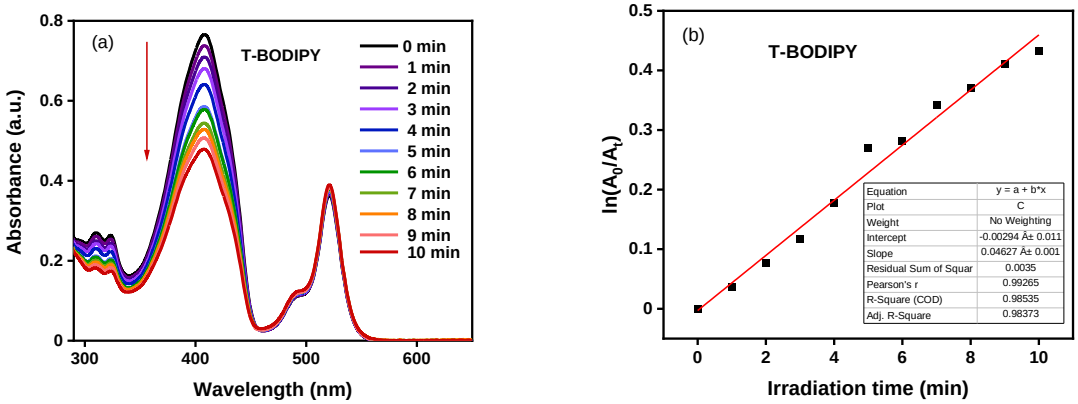

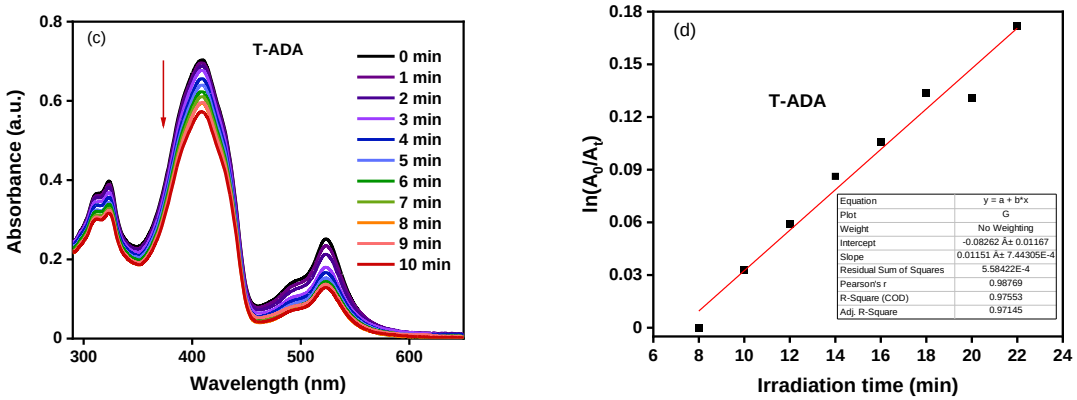

Figure S14. Changes in absorbance spectrum of DPBF upon irradiation in presence of (a) **T-BODIPY**, (c) **T-ADA**, in different interval of time and plot of change in absorption at A_0 and A_t with respect to irradiation time of (b) **T-BODIPY** and (d) **T-ADA** in MeOH. A_0 - absorbance at time = 0 min and A_t- absorbance at time = t.

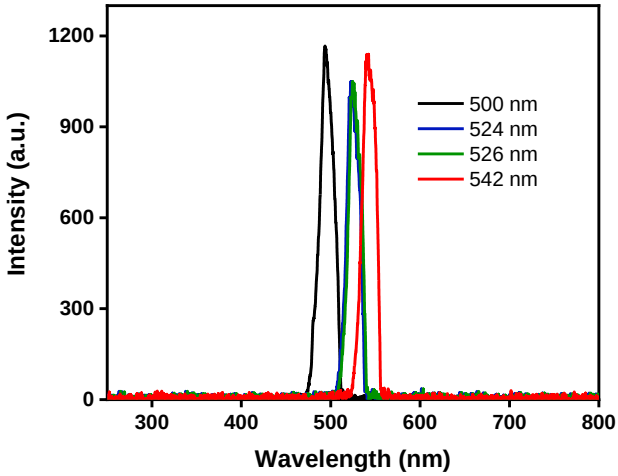

Figure S15. The spectrum of light source used for calculating the singlet oxygen quantum yields.

13. Femtosecond transient absorption (fs-TA) spectroscopy

Femtosecond transient absorption spectroscopy setup is described in detail elsewhere.[S13-S14] In brief, Ti: Sapphire regenerative amplified femtosecond laser (Libra, Coherent) delivered fundamental ~55 fs pulses centred at 800 nm at 1kHz repetition rate. A portion of 800 nm fundamental output was frequency doubled by a 0.5 mm BBO crystal (type-I) to produce 400 nm excitation pump pulses. White light continuum (WLC) probe pulses were generated using CaF_2 window (4mm thick, for visible region). Time-resolved transient absorption difference signal (ΔA) was obtained by chopping the pump pulse with the help of a synchronized mechanical chopper at half the repetition rate of the laser. The power the pump was attenuated

to 300 uW. To minimize the influence of anisotropic dynamics on the TA measurements, pump polarization was set at the magic angle to the vertically polarized probe set by using a half-wave plate (Thorlabs) and a Glan-laser polarizer (Thorlabs). The time delay between the pump and probe pulses is controlled using a mechanical delay stage (Newport). The pump and probe beams were focused onto a 1 mm path length sample quartz cuvette. Differential absorption spectra are collected by varying the pump-probe time delay keeping 1 sec integration time (i.e., averaging over 1000 laser shots). The data are collected in four different segments at different step sizes (-1 ps to +1 ps at 0.01 ps step-size, 1.1 ps to 10 ps at 0.1 ps step-size, 11 ps to 100 ps at 1 ps step-size, 101 ps to 3700 ps at 10 ps step-size). All the measurements are carried out at room temperature, and no photodegradation of the samples is noticed after the pump-probe measurements.

Global and target analysis of fs-TA data

The TA data is analysed globally to fit it with the singular value decomposition factors in the using a free R-package TIMP software with the graphical interface program Glotaran (version 1.5.1) software. Based on the statistical fitting package TIMP, we have analysed TA data using a kinetic model (global and target analysis).[S15-S16] We obtained (from global analysis) sequentially interconverting evolution associated difference spectra (EADS), *e.g.*, $1 \rightarrow 2 \rightarrow 3\ldots$; where the arrows indicate successive mono-exponential decays of increasing time constants, which can be regarded as the lifetime of each EADS. This procedure validates a depiction of the evolution of the (excited) states of the system. For obtaining the contributions from these molecular species (because the EADS may reflect mixtures of molecular species), a target analysis was performed in which a specific kinetic scheme was applied. We obtained the spectrum signature of the "pure" excited and product state intermediates as species-associated difference spectra (SADS). Each of these states can be ascribed to a distinct intermediate of the relaxation process.

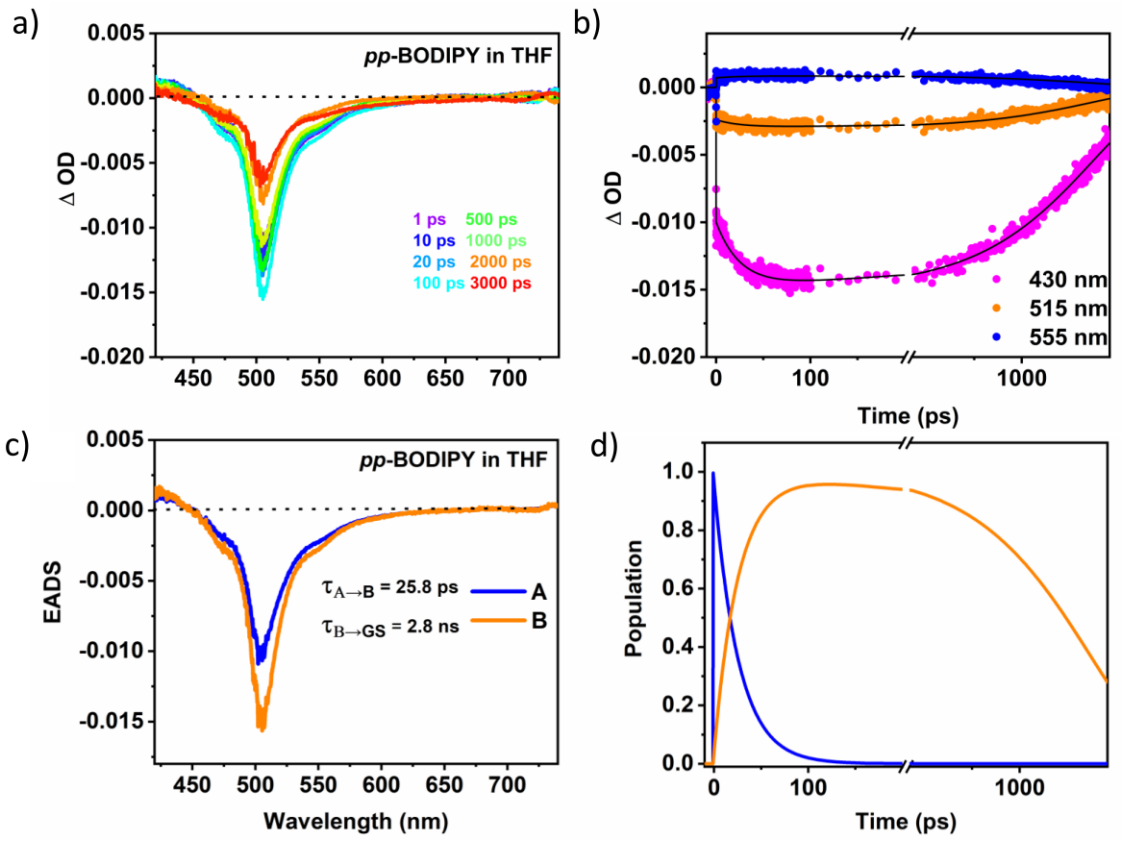

Figure S16. a) fs-TA spectral traces for ***pp*-BODIPY** in **THF** after photoexcitation at 400 nm at indicated probe delay time, b) Kinetic traces along with corresponding global fits at indicated probe wavelengths, c) Evolution associated difference spectra (EADS) reconstructed by singular value decomposition (SVD) and global fitting of **A** the transient data using sequential model A to B to GS (ground state), where **A** is ^{1}***pp*-BODIPY*,** and B is relaxed ^{1}***pp*-BODIPY** and d) Population dynamics for species A and B.

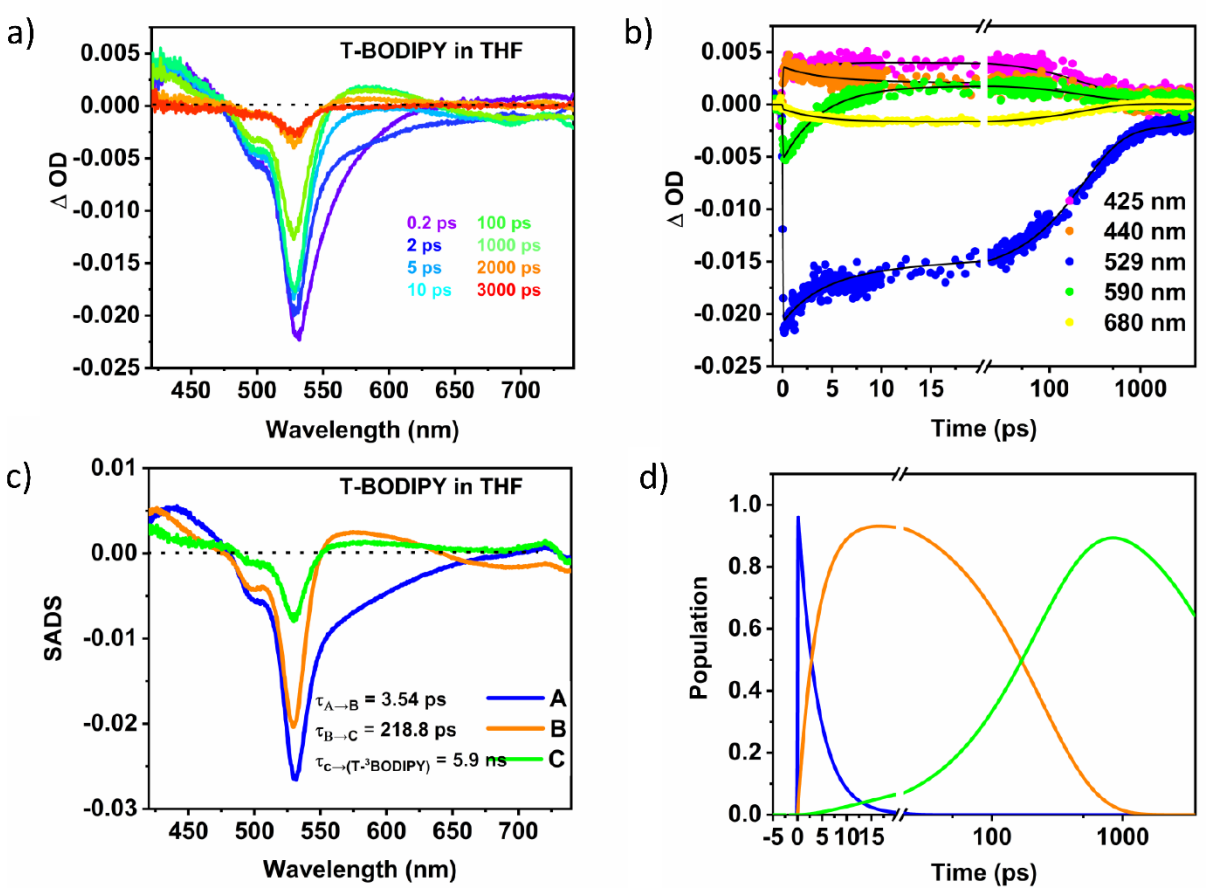

Figure S17. a) fs-TA spectral traces for **T-BODIPY** in THF after photoexcitation at 400 nm at indicated probe delay time, b) Kinetic traces along with corresponding global fits at indicated probe wavelengths, c) Species associated difference spectra (SADS) reconstructed by singular value decomposition (SVD) and global fitting of the transient data (global analysis) using target model (figure 8d), where **A** is **^{1}T-BODIPY*, B** is **^{1}(T$^{\cdot+}$-BODIPY $^{\cdot-}$) /^{1}CT** and **C** is **^{3}(T$^{\cdot+}$-BODIPY $^{\cdot-}$) / ^{3}CT** and d) Population dynamics for species A, B and C.

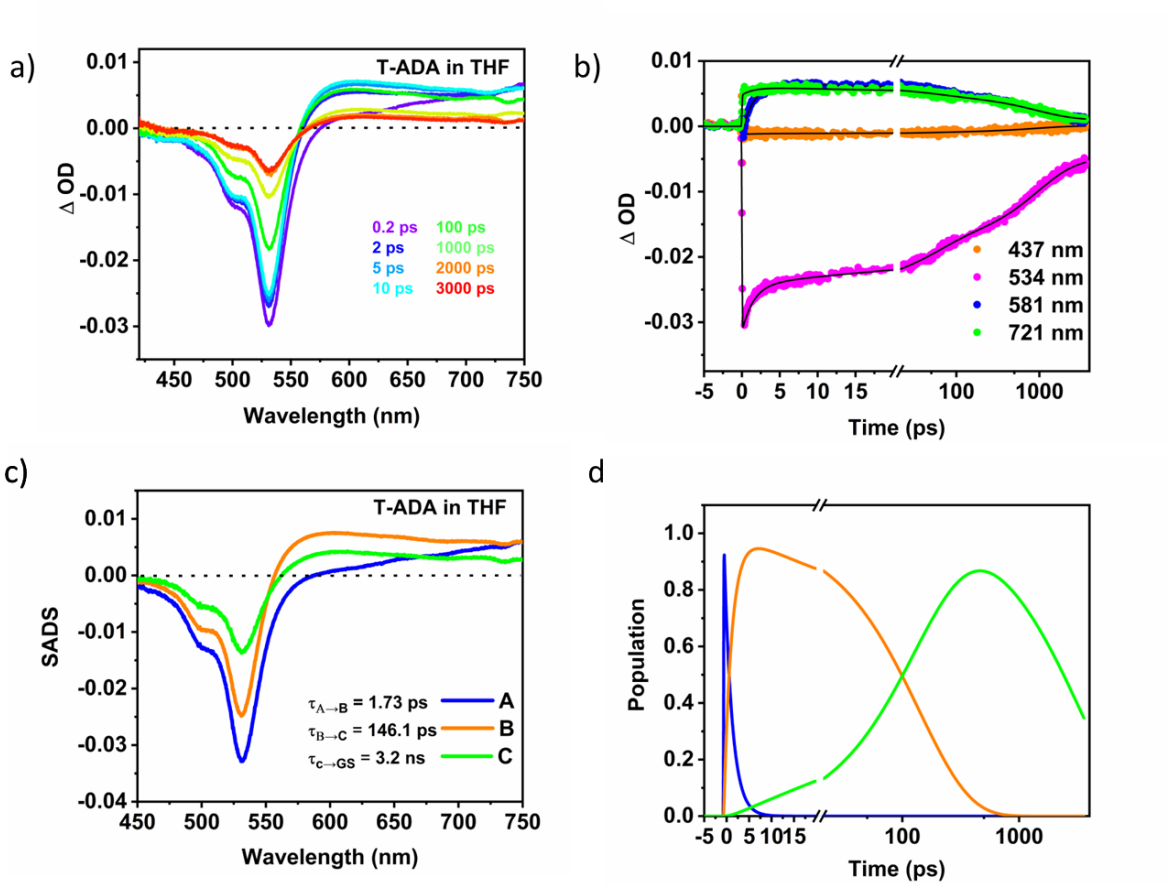

Figure S18. a) fs-TA spectral traces for **T-ADA** in THF after photoexcitation at 400 nm at indicated probe delay time, b) Kinetic traces along with corresponding global fits at indicated probe wavelengths, c) Species associated difference spectra (SADS) reconstructed by singular value decomposition (SVD) and global fitting of the transient data (global analysis) using target model (figure 8d), where **A** is ^{1}**BDT-BODIPY*, B** is ^{1}**(BDT$^{\cdot+}$-BODIPY$^{\cdot-}$) / ^{3}CT** and **C** is ^{3}**(BDT$^{\cdot+}$BODIPY$^{\cdot-}$) / ^{3}CT** and d) Population dynamics for species A, B and C.

14. Photocatalysis

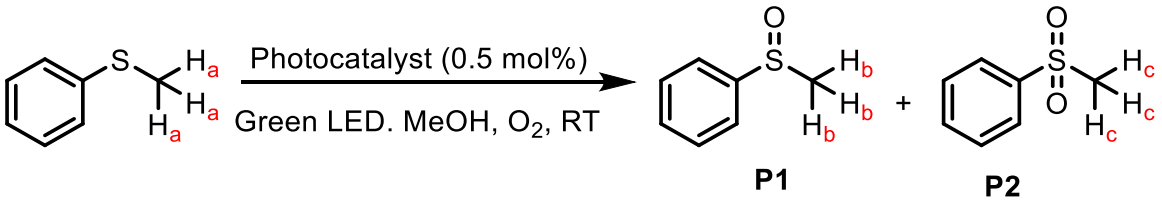

Scheme S10. Oxidation of thioanisole using ***pp*-BODIPY**, ***mp*-BODIPY**, ***mm*-BODIPY**, **T-BODIPY** and **T-ADA** as photocatalyst in MeOH in presence of oxygen.

Oxidation of Thioanisole catalyzed by BODIPYs:

***pp*-BODIPY as photocatalyst:** To a 10 mL vial equipped with a magnetic stir bar were added ***pp*-BODIPY** (1.92 mg, 0.0040 mmol, 0.005 equiv) catalyst, thioanisole (94.6 µL, 0.8050 mmol, 1.0 equiv) and methanol (2 mL). Next, a balloon was filled with oxygen and fixed on

the top of the vial. The reaction mixture was stirred and irradiated by green LED at room temperature under oxygen atmosphere. Aliquots were collected at equal time intervals and ^{1}H NMR was recorded to calculate the conversion yields based on the integration of NMR peaks of the substrate and product.

^{1}H NMR of crude mixture for oxidation of thioanisole using ***pp*-BODIPY**

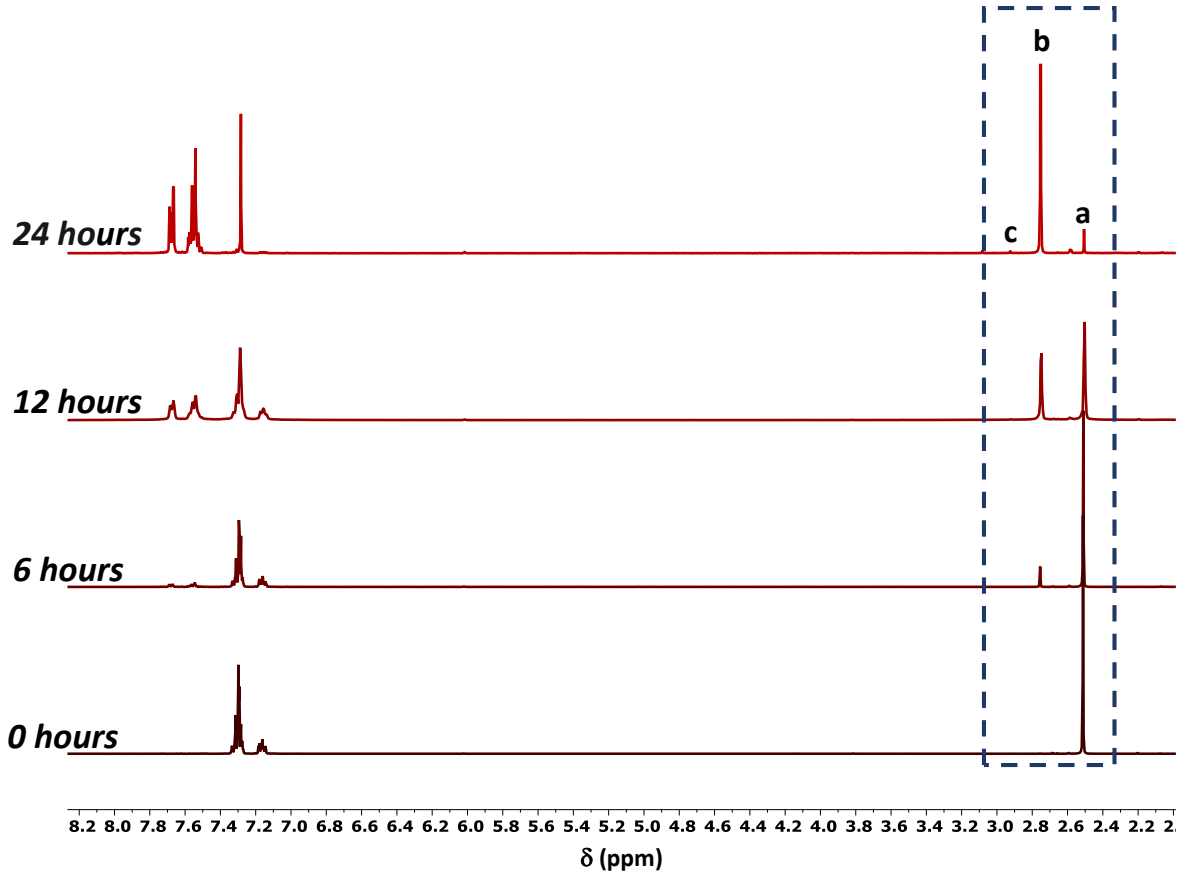

***mp*-BODIPY as photocatalyst**: To a 10 mL vial equipped with a magnetic stir bar were added ***mp*-BODIPY** (1.92 mg, 0.0040 mmol, 0.005 equiv) catalyst, thioanisole (94.6 µL, 0.8050 mmol, 1.0 equiv) and methanol (2 mL). Next, a balloon was filled with oxygen and fixed on the top of the vial. The reaction mixture was stirred and irradiated by green LED at room temperature under oxygen atmosphere. Aliquots were collected at equal time intervals and ^{1}H NMR was recorded to calculate the conversion yields based on the integration of NMR peaks of the substrate and product.

^{1}H NMR of crude mixture for oxidation of thioanisole using ***mp*-BODIPY**

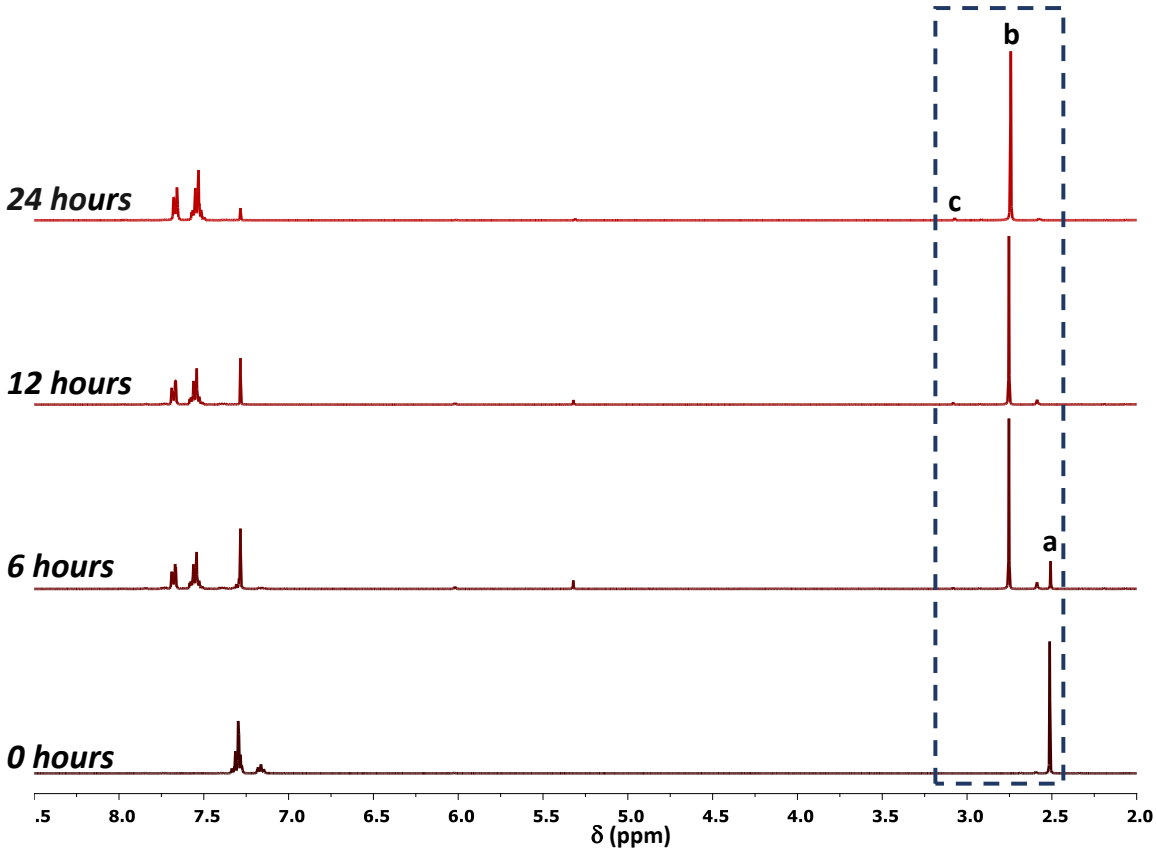

***mm*-BODIPY as photocatalyst:** To a 10 mL vial equipped with a magnetic stir bar were added ***mm*-BODIPY** (1.92 mg, 0.0040 mmol, 0.005 equiv) catalyst, thioanisole (94.6 µL, 0.8050 mmol, 1.0 equiv) and methanol (2 mL). Next, a balloon was filled with oxygen and fixed on the top of the vial. The reaction mixture was stirred and irradiated by green LED at room temperature under oxygen atmosphere. Aliquots were collected at equal time intervals and ^{1}H NMR was recorded to calculate the conversion yields based on the integration of NMR peaks of the substrate and product.

^{1}H NMR of crude mixture for oxidation of thioanisole using ***mm*-BODIPY**

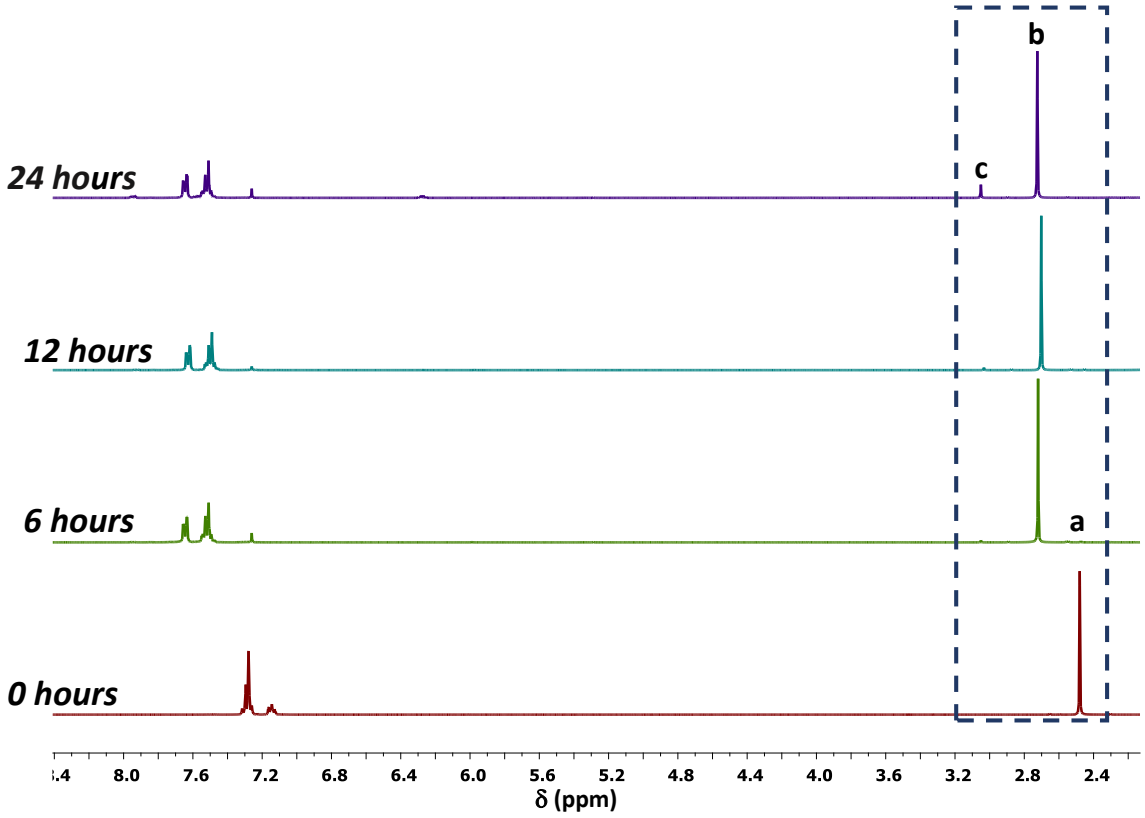

T-BODIPY as photocatalyst: To a 10 mL vial equipped with a magnetic stir bar were added **T-BODIPY** (1.53 mg, 0.0040 mmol, 0.005 equiv) catalyst, thioanisole (94.6 µL, 0.8050 mmol, 1.0 equiv) and methanol (2 mL). Next, a balloon was filled with oxygen and fixed on the top of the vial. The reaction mixture was stirred and irradiated by green LED at room temperature under oxygen atmosphere. Aliquots were collected at equal time intervals and ^{1}H NMR was recorded to calculate the conversion yields based on the integration of NMR peaks of the substrate and product.

^{1}H NMR of crude mixture for oxidation of thioanisole using **T-BODIPY**

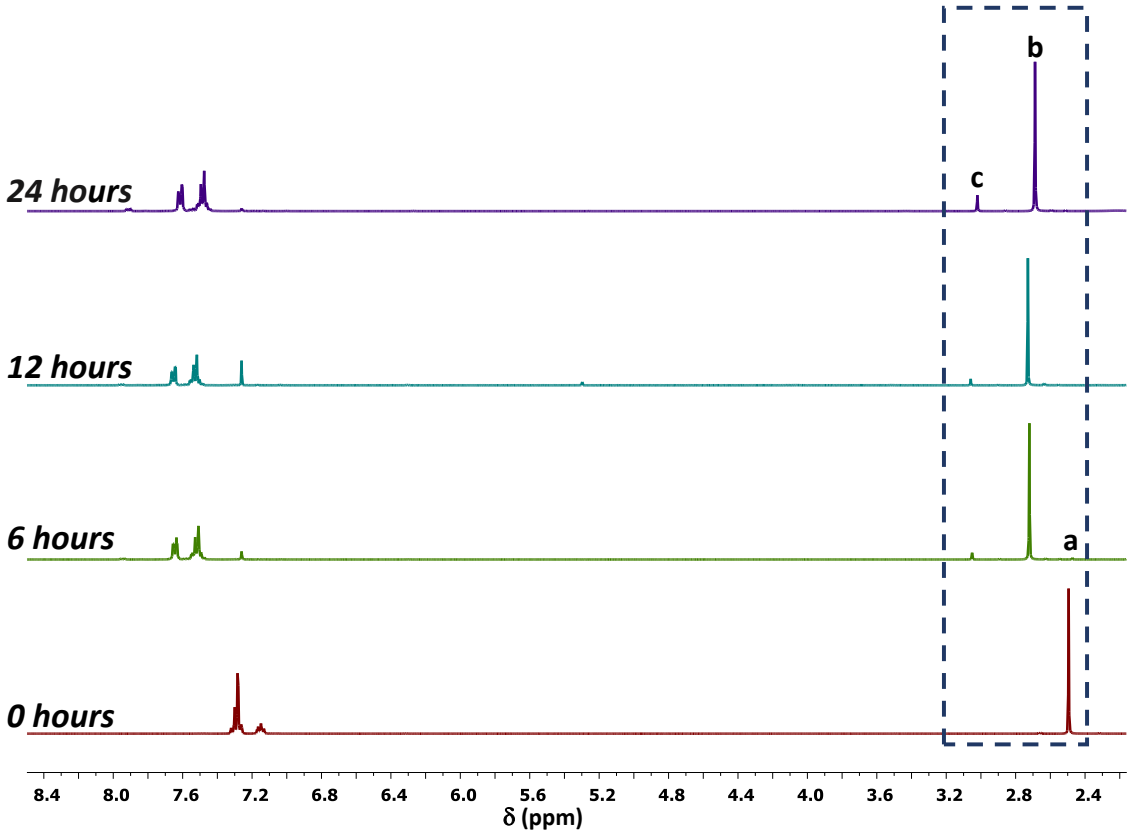

T-ADA as photocatalyst: To a 10 mL vial equipped with a magnetic stir bar were added **T-BODIPY** (3.70 mg, 0.0040 mmol, 0.005 equiv) catalyst, thioanisole (94.6 µL, 0.8050 mmol, 1.0 equiv) and methanol (2 mL). Next, a balloon was filled with oxygen and fixed on the top of the vial. The reaction mixture was stirred and irradiated by green LED at room temperature under oxygen atmosphere. Aliquots were collected at equal time intervals and ^{1}H NMR was recorded to calculate the conversion yields based on the integration of NMR peaks of the substrate and product.

^{1}H NMR of crude mixture for oxidation of thioanisole using **T-ADA**

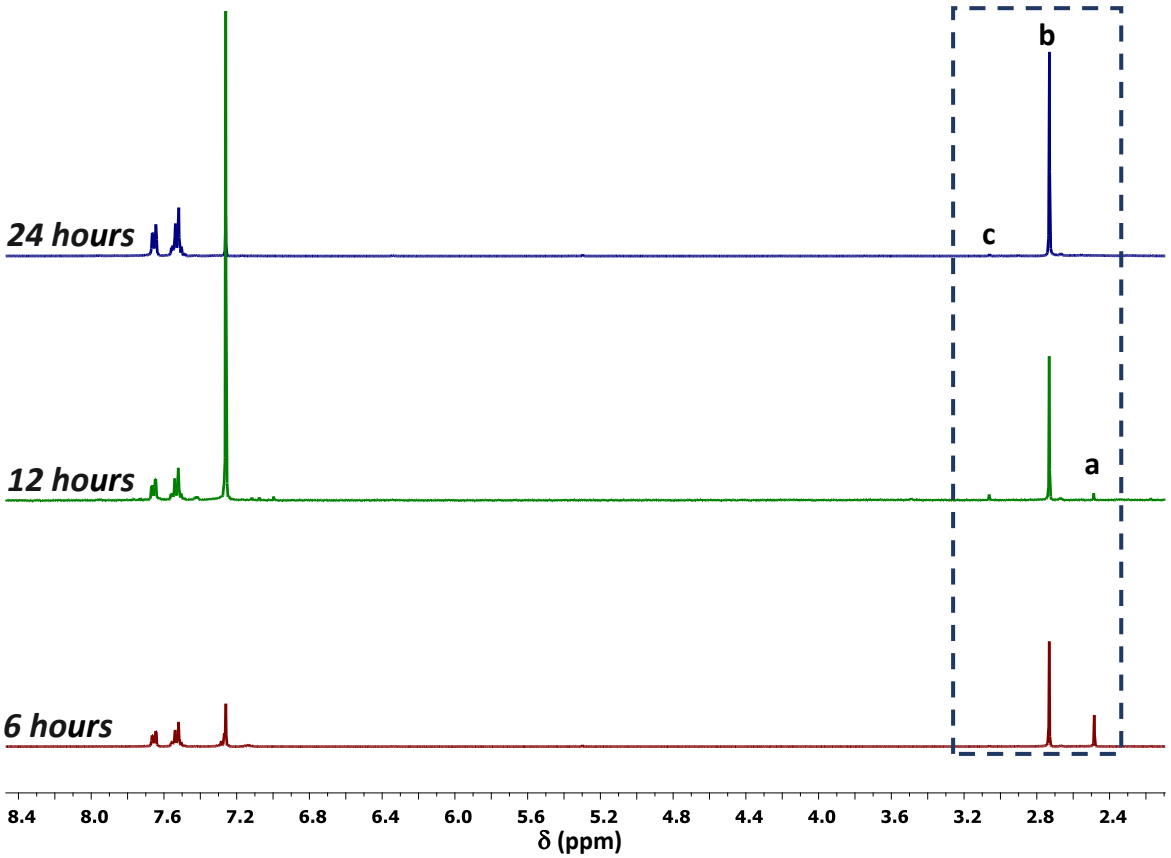

Control Experiment:

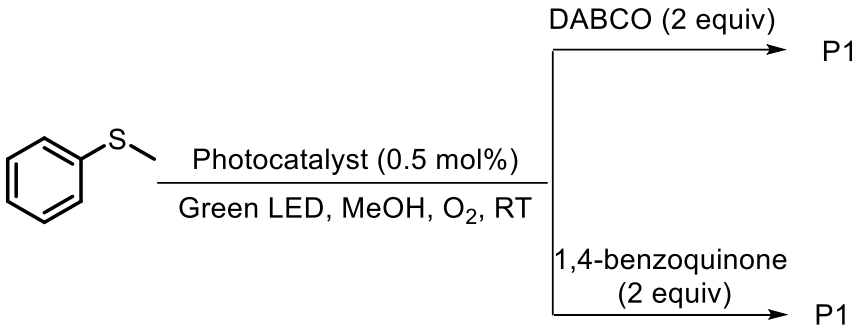

Scheme 11. Control experiments of oxidation of thioanisole using ***mp*-BODIPY** as photocatalyst.

Table S10. Control experiments of oxidation of thioanisole using ***mp*-BODIPY** as photocatalyst

Entry	Conditions	Conversion (P1, %)[a]
1	No light	0
2	No photocatalyst	0
3	DABCO	3
4	Benzoquinone	8

[a]Conversion was determined by ^{1}H NMR, All the reactions were performed at room temperature for 12 h taking ***mp*-BODIPY** photocatalyst.

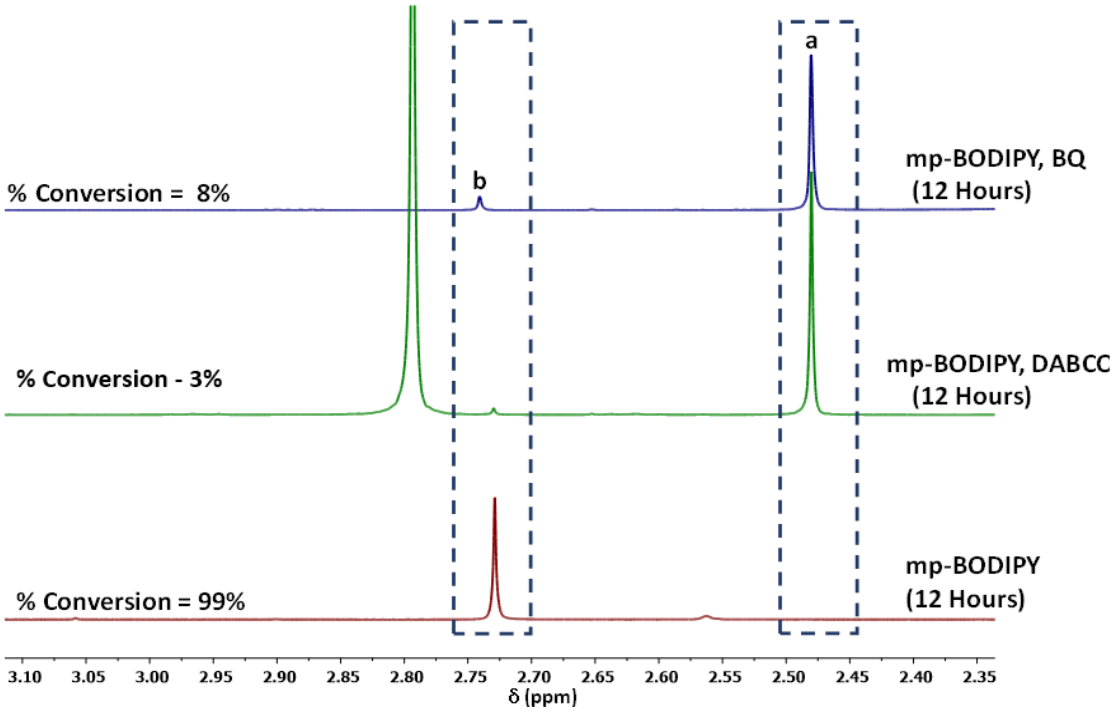

Table S11. Control experiments of oxidation of thioanisole using **T-BODIPY** as photocatalyst

Entry	Conditions	Conversion (P1, %)[a]
1	No light	0
2	No photocatalyst	0
3	DABCO	38
4	Benzoquinone	4

[a]Conversion was determined by ^{1}H NMR, all the reactions were performed at room temperature for 24 h taking **T-BODIPY** photocatalyst.

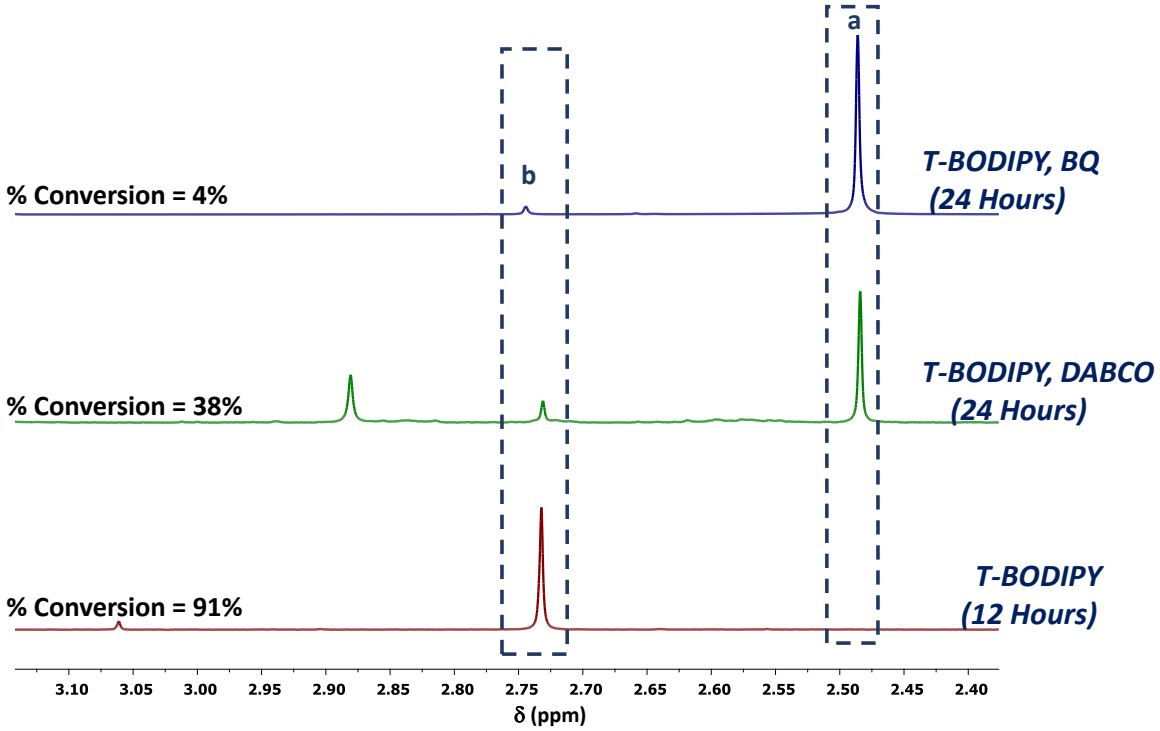

Table S12. Control experiments of oxidation of thioanisole using **T-ADA** as photocatalyst

Entry	Conditions	Conversion (P1, %)[a]
1	No light	0
2	No photocatalyst	0
3	DABCO	51
4	Benzoquinone	11

[a]Conversion was determined by ^{1}H NMR, all the reactions were performed at room temperature for 24 h taking **T-ADA** photocatalyst.

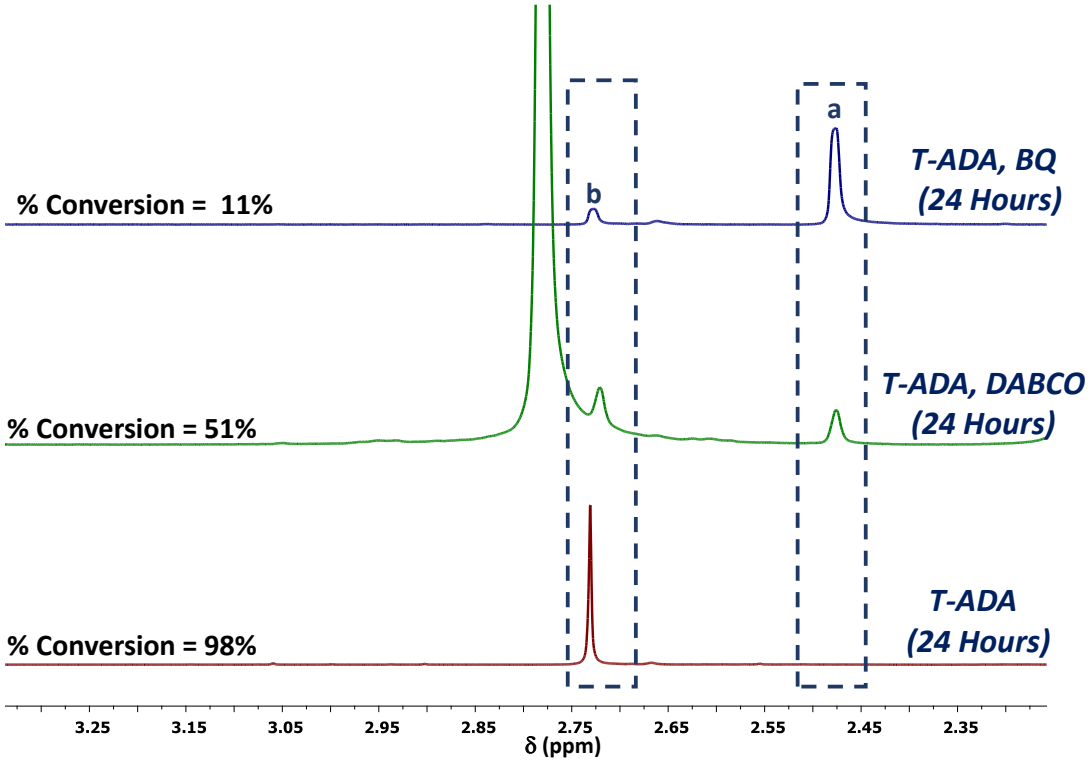

PDI as photocatalyst: The photooxidation of thioanisole was also performed using PDI as photocatalyst. The photocatalyst PDI was prepared following the procedure outlined in a previously published work.[S17] The photooxidation reaction was performed using similar condition as described in literature[S18] in our system using green LED in MeOH in oxygen atmosphere and observed comparable results. At intervals of 6, 12, 18, and 24 hours, conversion rates of 22%, 51%, 71%, and 94% were observed, respectively.

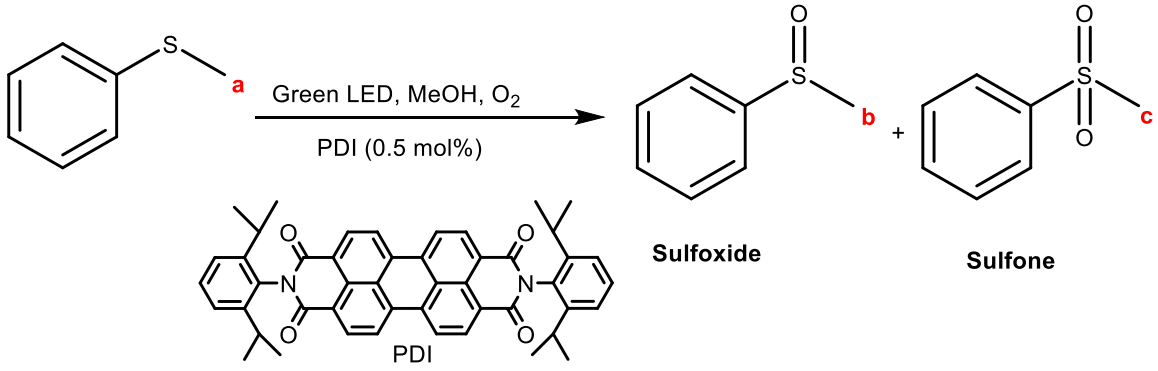

Scheme S12. Oxidation of thioanisole using **PDI** as photocatalyst in MeOH in presence of oxygen.

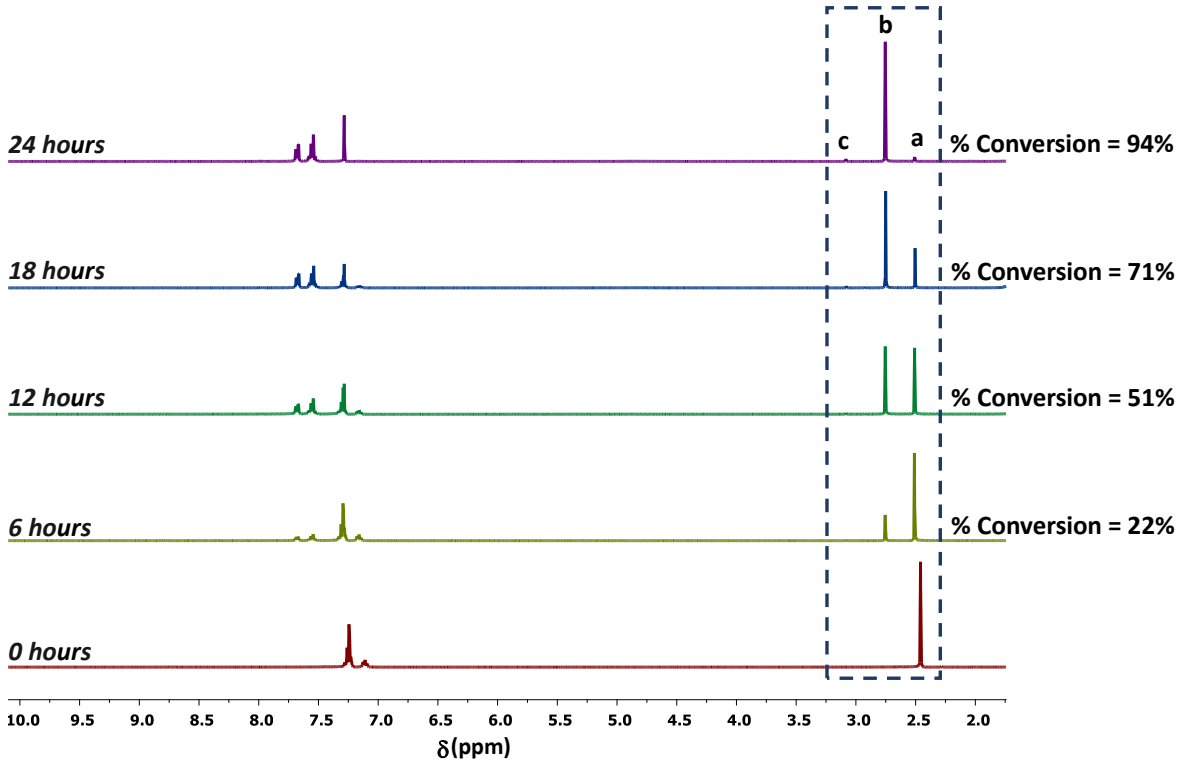

Table S13. Oxidation of thioanisole using various photocatalyst in MeOH in presence of oxygen.

S. No.	Photocatalyst	Loading (mol%)	Light Source	Conversion (%)	Time (h)	References
1.	pp-BODIPY	0.5	Green LED	95	24	Our Work
	mp-BODIPY	0.5	Green LED	99	24	
	mm-BODIPY	0.5	Green LED	92	24	
	T-BODIPY	0.5	Green LED	91	24	
	T-ADA	0.5	Green LED	99	24	
2.	PDI-1	2	5 W Blue LED	40	10	*Org. Biomol. Chem.*, 2019, **17**, 7144–7149.
	PDI-2	2	5 W Blue LED	Trace	10	
	PDI-3	2	5 W Blue LED	91	10	
3.	BODIPY 1	0.5	24 W household fluorescent light bulb	89	24	Catal. Commun., 2011, **16**, 94-97.
	BODIPY 2	0.5		99	24	
	BODIPY 3	0.5		99	24	
	BODIPY 4	0.5		99	24	
4.	BODIPY 1	0.5	24 W fluorescent lamp	100	24	*Catal. Letters*, 2014, **144**, 308-313
	BODIPY 2	0.5		8	24	
	BODIPY 3	0.5		28	24	
	BODIPY 4	0.5		13	24	
5.	PhBDP-2I	5	24 W household fluorescent lamp	100	3	*RSC Adv.*, 2013, **3**, 13417–13421.
	PhBDP			100	24	
	1I-PhBDP			100	24	

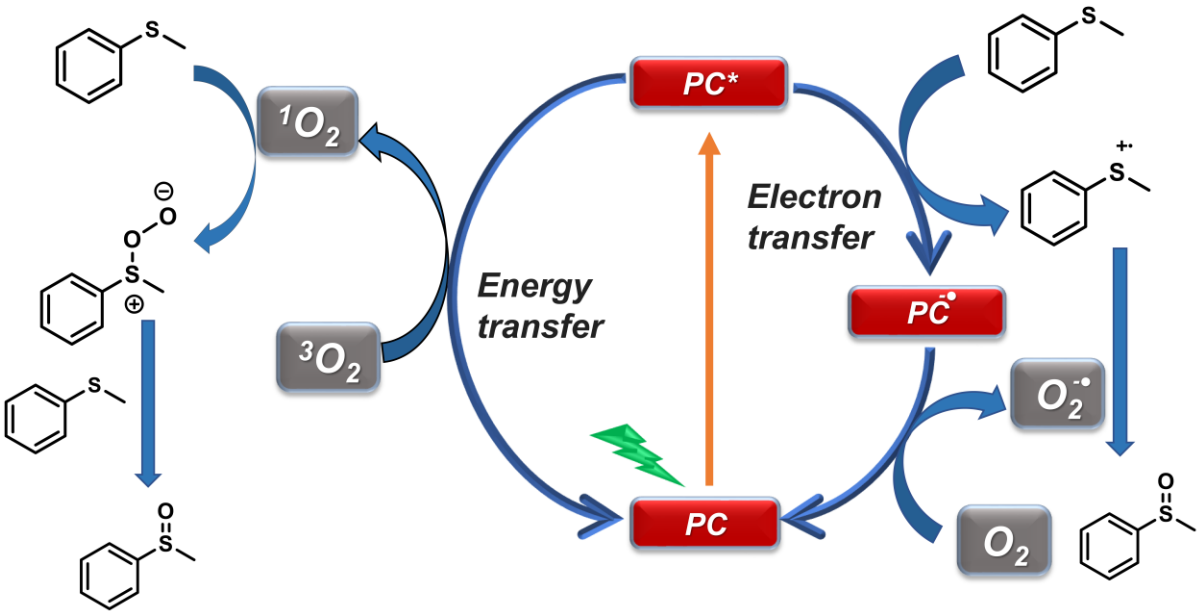

Scheme 12. Possible mechanistic pathways of photooxidation of thioanisole based on literature[S18-S20] and our control experiments.

Recyclability of T-ADA: To check the recyclability of catalyst, **T-ADA** was separated by column chromatography from the reaction mixture, dried, and utilized for next reaction with fresh substrates and solvent. There was 71% conversion and the NMR spectra is shown below.

^{1}H-NMR of reaction mixture recycling T-ADA

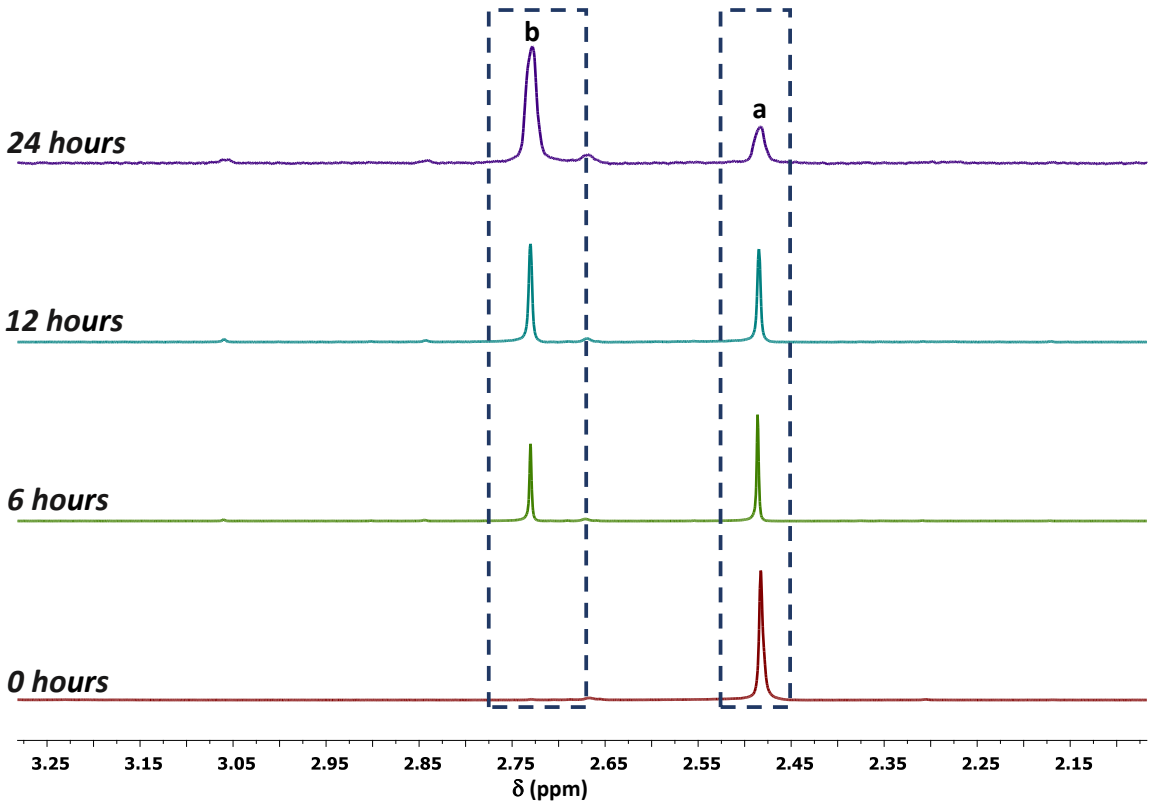

15. Frequencies and Coordinates of DFT Optimized Geometries

Table S14. Results of first three frequencies and molecular symmetries calculated from geometry optimization of ***pp*-BODIPY**, ***mp*-BODIPY**, ***mm*-BODIPY**, **T-BODIPY** and **T-ADA**.

Compounds	Symmetry	First Three Frequencies
		16.76
***pp*-BODIPY**	C_1	21.61
		22.45
		13.24
***mp*-BODIPY**	C_1	20.93
		24.47
		11.87
***mm*-BODIPY**	C_1	19.09
		27.23
		28.05
T-BODIPY	C_1	40.38
		54.08
		5.47
T-ADA	C_1	8.12
		10.71

Coordinates of geometry optimized structure of *pp*-BODIPY

C	-1.34781	0.03846	-1.20274
C	0.04523	0.03930	-1.20379
C	0.76033	-0.00005	-0.00005
C	0.04525	-0.03939	1.20372
C	-1.34778	-0.03853	1.20270
C	-2.07290	-0.00003	-0.00001
C	-3.55716	-0.00002	0.00001
C	-4.28109	-0.76195	0.93211
C	-5.67410	-0.76701	0.93855
C	-6.36105	-0.00001	0.00005
C	-5.67412	0.76698	-0.93847
C	-4.28111	0.76191	-0.93207
Br	-8.27208	0.00000	0.00008
C	2.25507	-0.00004	-0.00004
C	2.94500	-1.22260	-0.05053
N	4.34465	-1.24347	-0.05195
B	5.28074	0.00004	0.00011
N	4.34458	1.24353	0.05216
C	2.94491	1.22256	0.05048
C	4.75858	2.52367	0.10415
C	3.63114	3.37003	0.13754
C	2.48665	2.58227	0.10479
C	2.48682	-2.58233	-0.10504
C	3.63137	-3.37001	-0.13766
C	4.75875	-2.52360	-0.10399
F	6.07568	0.04808	-1.14365
F	6.07560	-0.04793	1.14393
C	1.08560	3.11787	0.12443
C	6.20313	2.90052	0.11969
C	1.08581	-3.11802	-0.12527
C	6.20335	-2.90034	-0.11938
H	-1.87998	0.04122	-2.14909
H	-6.22017	-1.36674	1.65769
H	0.58557	-0.06108	2.14551
H	-1.87993	-0.04128	2.14906
H	-3.74976	-1.38184	1.64760
H	-6.22021	1.36672	-1.65759
H	-3.74979	1.38180	-1.64758
H	3.66431	4.45051	0.18107
H	3.66460	-4.45049	-0.18125
H	1.10962	4.21026	0.16100
H	0.51955	2.76351	0.99130
H	0.51773	2.82176	-0.76281
H	6.31670	3.98529	0.16578
H	6.70586	2.52050	-0.77489
H	6.70659	2.44585	0.97828
H	1.10991	-4.21044	-0.16064
H	0.52055	-2.76466	-0.99308
H	0.51710	-2.82093	0.76109
H	6.70609	-2.51951	0.77484
H	6.70666	-2.44626	-0.97837
H	6.31701	-3.98513	-0.16466
H	0.58551	0.06099	-2.14559

Coordinates of geometry optimized structure of *mp*-BODIPY

C	1.63747	0.29229	0.76500
C	0.25947	0.13496	0.89553
C	-0.57901	0.22839	-0.22256
C	-0.00307	0.48224	-1.47388
C	1.37521	0.63820	-1.60270

C	2.22269	0.54687	-0.48625
C	3.69166	0.71520	-0.62643
C	4.57347	-0.07263	0.13189
C	5.94749	0.09489	-0.00606
C	6.48582	1.03057	-0.88637
C	5.61052	1.81255	-1.64082
C	4.23141	1.66023	-1.51442
Br	7.12624	-0.99876	1.03179
C	-2.05785	0.06095	-0.08362
C	-2.62296	-1.21793	-0.21766
N	-4.00594	-1.39483	-0.09242
B	-5.05170	-0.27709	0.19448
N	-4.24447	1.04961	0.31173
C	-2.85769	1.18567	0.17844
C	-4.77709	2.26168	0.55693
C	-3.74298	3.21984	0.58882
C	-2.53497	2.57354	0.35515
C	-2.03887	-2.50364	-0.47797
C	-3.09568	-3.40588	-0.49956
C	-4.29259	-2.69969	-0.26018
F	-5.71584	-0.53982	1.39121
F	-5.96100	-0.19160	-0.85838
C	-1.20035	3.25704	0.31110
C	-6.24251	2.47036	0.75187
C	-0.60106	-2.87401	-0.69194
C	-5.68585	-3.23130	-0.18817
H	2.26468	0.24183	1.64978
H	-0.63941	0.54841	-2.35139
H	1.80194	0.80760	-2.58651
H	4.19004	-0.82927	0.80634
H	7.55969	1.14353	-0.97793
H	6.01212	2.55327	-2.32573
H	3.56556	2.29615	-2.08881
H	-3.87958	4.27827	0.76636
H	-3.02466	-4.47191	-0.66977
H	-1.33024	4.32926	0.48049
H	-0.70029	3.12524	-0.65322
H	-0.51502	2.87554	1.07417
H	-6.45928	3.52430	0.93621
H	-6.60407	1.87260	1.59411
H	-6.79605	2.13461	-0.13031
H	-0.51916	-3.95164	-0.85671
H	0.02476	-2.61515	0.16750
H	-0.16803	-2.36625	-1.55921
H	-6.31912	-2.74291	-0.93505
H	-6.12781	-3.01137	0.78841
H	-5.69460	-4.31010	-0.35504
H	-0.17317	-0.05322	1.87365

Coordinates of geometry optimized structure of *mm*-BODIPY

C	-0.82907	0.79396	0.60598
C	0.42299	1.01361	1.18950
C	0.51138	1.77835	2.35960
C	-0.64455	2.31077	2.93098
C	-1.88867	2.08617	2.34523
C	-2.00065	1.32359	1.17103
C	-3.32503	1.08640	0.53987
C	-3.62480	-0.15557	-0.04383
C	-4.86815	-0.36408	-0.63202
C	-5.84053	0.63293	-0.66005
C	-5.54355	1.86668	-0.08016

C	-4.30311	2.09412	0.51205
Br	-5.25449	-2.06892	-1.40990
C	1.65630	0.44584	0.56177
C	2.11467	-0.81934	0.96446
N	3.26935	-1.36594	0.39218
B	4.15599	-0.69909	-0.70088
N	3.49328	0.67475	-1.01523
C	2.33642	1.18843	-0.41738
C	3.95271	1.57007	-1.90974
C	3.10071	2.69372	-1.91407
C	2.08403	2.48047	-0.99092
C	1.61083	-1.76433	1.92104
C	2.48432	-2.84472	1.88723
C	3.49384	-2.57504	0.94030
F	5.44832	-0.50641	-0.21574
F	4.17963	-1.49198	-1.84666
C	0.97788	3.45283	-0.70592
C	5.17964	1.33221	-2.72639
C	0.40296	-1.67614	2.80611
C	4.65259	-3.43139	0.54925
H	-0.88721	0.22283	-0.31554
H	1.48135	1.95230	2.81525
H	-0.57571	2.89641	3.84290
H	-2.78396	2.48251	2.81384
H	-2.90184	-0.96251	-0.01862
H	-6.80250	0.44811	-1.12351
H	-6.28612	2.65867	-0.10089
H	-4.07951	3.06858	0.93401
H	3.22765	3.56946	-2.53648
H	2.41195	-3.74600	2.48126
H	1.11478	4.35327	-1.31063
H	0.95131	3.75222	0.34615
H	-0.00715	3.03687	-0.93905
H	5.37157	2.17970	-3.38721
H	5.06897	0.42282	-3.32476
H	6.04572	1.17529	-2.07619
H	0.31605	-2.58812	3.40264
H	-0.52175	-1.55869	2.23294
H	0.45500	-0.82637	3.49352
H	4.64774	-4.36557	1.11407
H	5.59425	-2.90355	0.72824
H	4.61761	-3.65419	-0.52149

Coordinates of geometry optimized structure of T-BODIPY

H	-0.68307	2.61760	0.55566
H	-0.14180	-3.07625	-0.03133
C	-1.07701	-0.34105	0.37142
C	-1.72334	-1.21697	1.21584
C	-3.14196	-1.17443	1.11976
C	-3.56176	-0.26756	0.18559
S	-2.24485	0.56134	-0.58328
H	-1.18851	-1.85279	1.91069
H	-3.81724	-1.77849	1.71203
Br	-5.33786	0.12662	-0.29502
C	0.36856	-0.15504	0.20770
C	1.18730	-1.29222	0.06592
N	2.57238	-1.17589	-0.03672
B	3.37627	0.16260	-0.08424
N	2.31465	1.30366	0.02920
C	0.94102	1.13141	0.19683
C	2.59085	2.62435	0.08497

C	1.39029	3.34146	0.29336
C	0.36174	2.41613	0.37465
C	0.85793	-2.66941	-0.03885
C	2.04932	-3.36315	-0.18134
C	3.09615	-2.41202	-0.18283
F	4.05837	0.26227	-1.29237
F	4.25962	0.22894	0.98827
C	3.97930	3.15615	-0.04554
C	4.56249	-2.64481	-0.33549
H	1.31543	4.41624	0.38115
H	2.18007	-4.43071	-0.28984
H	4.43191	2.81754	-0.98233
H	4.61045	2.77492	0.76339
H	3.97692	4.24734	-0.01740
H	4.77824	-3.71353	-0.38885
H	5.10859	-2.20558	0.50489
H	4.93377	-2.15492	-1.24104

Coordinates of geometry optimized structure of T-ADA

C	-1.16710	0.78953	-0.50634
C	-1.22735	-0.63033	-0.50369
C	-0.08977	-1.44960	-0.50247
C	1.16709	-0.78961	-0.50638
C	1.22735	0.63024	-0.50363
C	0.08977	1.44952	-0.50235
C	2.46657	-1.38340	-0.49766
C	3.48985	-0.47164	-0.49968
S	2.88866	1.19495	-0.51321
C	-2.46657	1.38332	-0.49762
C	-3.48985	0.47155	-0.49972
S	-2.88866	-1.19504	-0.51334
C	0.19072	2.86749	-0.49775
C	-0.19072	-2.86758	-0.49798
C	0.29464	4.07674	-0.49257
C	-0.29460	-4.07683	-0.49291
C	0.42591	5.52842	-0.48504
C	-0.42587	-5.52852	-0.48541
C	4.90973	-0.75687	-0.50592
C	-4.90973	0.75679	-0.50600
C	5.53510	-1.91539	-0.92794
C	6.94022	-1.88459	-0.77603
C	7.41941	-0.69705	-0.25817
S	6.09071	0.39620	0.07550
C	-5.53508	1.91528	-0.92810
C	-6.94020	1.88451	-0.77620
C	-7.41941	0.69701	-0.25826
S	-6.09073	-0.39622	0.07549
C	8.81162	-0.34504	0.02711
C	-8.81163	0.34505	0.02704
C	9.62500	-1.28209	0.69674
N	10.97332	-1.02608	0.93816
B	11.72892	0.29549	0.59159
N	10.67232	1.22922	-0.08051
C	9.34685	0.89948	-0.36190
C	-9.62499	1.28220	0.69656
N	-10.97331	1.02624	0.93799
B	-11.72895	-0.29535	0.59157
N	-10.67235	-1.22920	-0.08037
C	-9.34687	-0.89952	-0.36178
C	9.31418	-2.54423	1.26705
C	10.48389	-3.03961	1.82285

C	11.49550	-2.07542	1.60981	H	0.00603	-5.97100	-1.39020
C	10.92603	2.45556	-0.58671	H	4.99446	-2.74760	-1.36249
C	9.75946	2.94920	-1.21346	H	7.59788	-2.68924	-1.08076
C	8.77688	1.97959	-1.08665	H	-4.99443	2.74746	-1.36271
C	-9.31415	2.54438	1.26676	H	-7.59786	2.68914	-1.08101
C	-10.48384	3.03983	1.82251	H	8.33713	-3.00267	1.27848
C	-11.49547	2.07564	1.60956	H	10.61928	-3.97755	2.34302
C	-10.92606	-2.45562	-0.58637	H	9.67644	3.90787	-1.70599
C	-9.75949	-2.94937	-1.21303	H	7.77014	2.01810	-1.47350
C	-8.77689	-1.97975	-1.08636	H	-8.33709	3.00281	1.27812
C	12.92472	-2.11760	2.03826	H	-10.61921	3.97783	2.34258
C	12.26473	3.10573	-0.47201	H	-9.67647	-3.90811	-1.70541
F	12.76620	0.03541	-0.29868	H	-7.77016	-2.01833	-1.47320
F	12.21472	0.88256	1.75577	H	13.15326	-3.07007	2.52018
C	-12.92465	2.11781	2.03817	H	13.13874	-1.29977	2.73335
C	-12.26474	-3.10579	-0.47154	H	13.58612	-1.97856	1.17763
F	-12.76617	-0.03536	-0.29881	H	12.24368	4.10701	-0.90633
F	-12.21484	-0.88222	1.75580	H	13.02439	2.50589	-0.98305
H	2.62116	-2.45465	-0.46337	H	12.57000	3.17064	0.57664
H	-2.62117	2.45456	-0.46330	H	-13.15360	3.07099	2.51849
H	0.01953	5.96872	-1.40266	H	-13.13812	1.30110	2.73476
H	1.47718	5.82552	-0.40874	H	-13.58610	1.97689	1.17790
H	-0.10912	5.97042	0.36300	H	-12.24382	-4.10696	-0.90610
H	-1.47883	-5.82560	-0.43772	H	-13.02450	-2.50579	-0.98226
H	0.08531	-5.96833	0.37835	H	-12.56980	-3.17095	0.57717

16. References:

S1. Gaussian 09, Revision C.01, M. J. Frisch, G. W. Trucks, H. B. Schlegel, G. E. Scuseria, M. A. Robb, J. R. Cheeseman, G. Scalmani, V. Barone, B. Mennucci, G. A. Petersson, H. Nakatsuji, M. Caricato, X. Li, H. P. Hratchian, A. F. Izmaylov, J. Bloino, G. Zheng, J. L. Sonnenberg, M. Hada, M. Ehara, K. Toyota, R. Fukuda, J. Hasegawa, M. Ishida, T.

Nakajima, Y. Honda, O. Kitao, H. Nakai, T. Vreven, J. A. Montgomery, Jr., J. E. Peralta, F. Ogliaro, M. Bearpark, J. J. Heyd, E. Brothers, K. N. Kudin, V. N. Staroverov, T. Keith, R. Kobayashi, J. Normand, K. Raghavachari, A. Rendell, J. C. Burant, S. S. Iyengar, J. Tomasi, M. Cossi, N. Rega, J. M. Millam, M. Klene, J. E. Knox, J. B. Cross, V. Bakken, C. Adamo, J. Jaramillo, R. Gomperts, R. E. Stratmann, O. Yazyev, A. J. Austin, R. Cammi, C. Pomelli, J. W. Ochterski, R. L. Martin, K. Morokuma, V. G. Zakrzewski, G. A. Voth, P. Salvador, J. J. Dannenberg, S. Dapprich, A. D. Daniels, O. Farkas, J. B. Foresman, J. V. Ortiz, J. Cioslowski, and D. J. Fox, Gaussian, Inc., Wallingford CT, 2010.

S2. D. Simoni, G. Giannini, M. Roberti, R. Rondanin, R. Baruchello, M. Rossi, G. Grisolia, F. P. Invidiata, S. Aiello, S. Marino, S. Cavallini, A. Siniscalchi, N. Gebbia, L. Crosta, S. Grimaudo, V. Abbadessa, A. Di Cristina and M. Tolomeo, *J. Med. Chem.*, 2005, **48**, 4293–4299.

S3. H. Bonin, D. Delbrayelle, P. Demonchaux and E. Gras, *Chem. Commun.*, 2010, **46**, 2677–2679.

S4. C. Thivierge, A. Loudet and K. Burgess, *Macromolecules*, 2011, **44**, 4012–4015.

S5. M. Ozdemir, D. Choi, G. Kwon, Y. Zorlu, B. Cosut, H. Kim, A. Facchetti, C. Kim, and H. Usta, *Acs appl.Mater. Interfaces,* 2016, **8**, 14077-14087.

S6. M. Yilmaz, M. Erkartal, M. Ozdemir, U. Sen, H. Usta and G. Demirel, *ACS Appl. Mater. Interfaces*, 2017, **9**, 18199–18206.

S7. S. Sharma, Z. Wei, F. C. Grozema and S. Sengupta, *Phys. Chem. Chem. Phys.*, 2020, **22**, 25514–25521.

S8. F. Liu, T. Wu, J. Cao, S. Cui, Z. Yang, X. Qiang, S. Sun, F. Song, J. Fan, J. Wang and X. Peng, *Chem. Eur. J.*, 2013, **19**, 1548–1553.

S9. K. Chen, W. Yang, Z. Wang, A. Iagatti, L. Bussotti, P. Foggi, W. Ji, J. Zhao and M. Di Donato, *J. Phys. Chem. A*, 2017, **121**, 7550–7564.

S10. V. Bandi, H. B. Gobeze, V. Lakshmi, M. Ravikanth, and F. D'Souza, J. Phys. Chem. C, 2015, **119**, 8095−8102.

S11. F. Zieschang, M. H. Schreck, A. Schmiedel, M. Holzapfel, J. H. Klein, C. Walter, B. Engels, C. Lambert, J. Phys. Chem. C., 2014, **118**, 27698−27714.

S12. N. Adarsh, R. R. Avirah and D. Ramaiah, *Org. Lett.*, 2010, **12**, 5720–5723.

S13. G. Bhutani, P. Verma, A. Jayachandran, S. Paul, K. Chattopadhyay and A. K. De, *J. Phys. Chem. B*, 2023, **127**, 3197–3207.

S14. Y. Silori, S. Chawla and A. K. De, *ChemPhysChem*, 2020, **21**, 1908–1917.

S15. I. H. M. Van Stokkum, D. S. Larsen and R. Van Grondelle, *Biochim. Biophys. Acta - Bioenerg.*, 2004, **1657**, 82–104.

S16. J. J. Snellenburg, S. Laptenok, R. Seger, K. M. Mullen and I. H. M. van Stokkum, *J. Stat. Softw.*, 2012, **49**, 1–22.

S17. C. Ramanan, A. L. Smeigh, J. E. Anthony, T. J. Marks, and M. R. Wasielewski, *J. Am. Chem. Soc.*, 2012, 134, 386–397.

S18. Y. Gao, H. Xu, S. Zhang, Y. Zhang, C. Tang and W. Fan, *Org. Biomol. Chem.*, 2019, **17**, 7144–7149.

S19. E. Baciocchi, T. Del Giacco, F. Elisei, M. F. Gerini, M. Guerra, A. Lapi and P. Liberali, *J. Am. Chem. Soc.*, 2003, **125**, 16444–16454.

S20. S. M. Bonesi, M. Fagnoni and A. Albini, *Eur. J. Org. Chem.*, 2008, **2008**, 2612–2620.